Observation and modelling of ozone-destructive halogen chemistry in a passive degassing volcanic plume

Luke Surl[1,2], Tjarda Roberts[1], and Slimane Bekki[2]

[1]CNRS, Laboratoire de Physique et de Chimie de l'Environnement et de l'Espace, Université d'Orléans, Orléans, France
[2]LATMOS/IPSL, Sorbonne Université, UVSQ, CNRS, Paris, France

Correspondence: Luke Surl (luke.surl@cnrs-orleans.fr)

Abstract.

Volcanoes emit halogens into the atmosphere that undergo complex chemical cycling in plumes and cause destruction of ozone. We present a case study of the Mount Etna plume in the summer of 2012, when the volcano was passively degassing, using aircraft observations and numerical simulations with a new 3D model "WRF-Chem Volcano" (WCV), incorporating volcanic emissions and multi-phase halogen chemistry.

Measurements of SO_2 — an indicator of plume intensity — and ozone were made in the plume a few 10s of km from Etna, revealing a strong negative correlation between ozone and SO_2 levels. From these observations, using SO_2 as a tracer species, we estimate a mean in-plume ozone loss rate of 1.3×10^{-5} molecules of O_3 per second per molecule of SO_2. This value is similar to observation-based estimates reported very close to Etna's vents, indicating continual ozone loss in the plume up to at least 10's km downwind.

The WCV model is run with nested grids to simulate the plume close to the volcano at 1 km resolution. The focus is on the early evolution of passively degassing plumes aged less than one hour and up to 10s km downwind. The model is able to reproduce the so-called 'bromine explosion': the daytime conversion of HBr into bromine radicals that continuously cycle in the plume. These forms include the radical BrO, a species whose ratio with SO_2 is commonly measured in volcanic plumes as an indicator of halogen ozone-destroying chemistry.

The species BrO is produced in the ambient temperature chemistry, with in-plume BrO/SO_2 ratios of order 10^{-4} mol/mol, similar to those observed previously in Etna plumes. Windspeed and time-of-day are identified as non-linear controls on this ratio. Sensitivity simulations confirm the importance of near-vent radical products from high temperature chemistry in initiating the ambient temperature plume halogen cycling. Heterogeneous reactions that activate bromine also activate a small fraction of the emitted chlorine; the resulting production of chlorine radical Cl strongly enhances the methane oxidation and hence the formation of formaldehyde (HCHO) in the plume.

Modelled rates of ozone depletion are found to be similar to those derived from aircraft observations. Ozone destruction in the model is controlled by the processes that recycle bromine, with about three-quarters of this recycling occurring via reactions between halogen oxide radicals. Through sensitivity simulations, a relationship between the magnitude of halogen emissions and ozone loss is established.

Volcanic halogens cycling impacts profoundly the overall plume chemistry in the model, notably hydrogen oxide radicals (HO_x), nitrogen oxides (NO_x), sulfur, and mercury chemistry. In the model, it depletes HO_x within the plume, increasing the lifetime of SO_2 and hence slowing sulfate aerosol formation. Halogen chemistry also promotes the conversion of NO_x into nitric acid (HNO_3). This, along with the displacement of nitrate out of background aerosols in the plume, results in enhanced HNO_3 levels and an almost total depletion of NO_x in the plume. The halogen-mercury model scheme is simple but includes newly-identified photo-reductions of mercury halides. With this set-up, the mercury oxidation is found to be slow and in near-balance with the photo-reduction in the plume. Overall, the model findings demonstrate that halogen chemistry has to be considered for a complete understanding of sulfur, HO_x, reactive nitrogen, and mercury chemistry, and of the formation of sulfate particles in volcanic plumes.

1 Introduction

1.1 Background

Volcanoes emit mixtures of various gases and particulates into the atmosphere. Of the gaseous emissions, H_2O, CO_2, and SO_2 are typically the species with the greatest fluxes. Most studies on the atmospheric impact of volcanic emissions have focused on sulfur because of its well-known effects on atmospheric composition, notably aerosol loading and climate (e.g. Oppenheimer et al., 2011). Several other species are emitted from volcanoes, including other sulphur species (such as H_2S, which can, in some cases, be dominant) and the primary focus of this study: halogens. Chlorine, bromine, and fluorine are routinely detected in various proportions within volcanic plumes, and are emitted primarily as hydrogen halides. Gerlach (2004) reported that gaseous emissions from arc volcanoes are, on average, 0.84% HCl, 0.061% HF, and 0.0025% HBr. Iodine has also been detected in volcanic plumes (e.g Aiuppa et al., 2005; Bobrowski et al., 2017), but its emission fluxes are typically about two orders of magnitude below those of bromine.

The quantities of halogen species emitted from a volcano and their temporal variability appear to provide information on sub-surface processes (Pyle and Mather, 2009). Correlations between the bromine-to-sulfur ratio and volcanic activity have been found in long-term observations (e.g. Bobrowski and Giuffrida, 2012; Dinger et al., 2018; Warnach et al., 2019; Dinger et al., 2020), suggesting that this ratio could potentially be used for monitoring and forecasting of volcanic activity.

However, volcanic halogen emissions are not just potential indicators of sub-surface processes. Importantly, they impact the chemical composition of the atmosphere and hence possibly the climate. For instance ozone, the precursor of the most important atmospheric oxidant (the hydrogen oxide radical OH), is found to be greatly depleted in volcanic plumes containing halogens (Rose et al., 2006; Vance et al., 2010; Kelly et al., 2013; Surl et al., 2015). Ozone is predominately destroyed by bromine chemistry cycles (Bobrowski et al., 2007; von Glasow, 2010; Roberts, 2018). Halogen chemistry also leads to the depletion of nitrogen oxides (NO_x) and hydrogen oxide radicals (HO_x) (Bobrowski et al., 2007; Roberts et al., 2009; Jourdain et al., 2016), and may oxidise mercury to more soluble, and therefore more easily deposited, forms (von Glasow, 2010). The effects are not limited to the troposphere because volcanic plumes can also reach the tropopause region, sometimes injecting halogens directly into the stratosphere (Rose et al., 2006; Millard et al., 2006). In the case of bromine- or chlorine-rich, large-

scale eruptions, this could result in massive stratospheric ozone depletion (Kutterolf et al., 2013; Cadoux et al., 2015; Brenna et al., 2020), dependent upon the fraction of emitted halogens that avoid dry- and wet-removal processes within the tropospheric plume and are therefore able to reach the stratosphere. Estimates for this fraction vary substantially (between 0 and 1) and it likely depends on both volcanic and atmospheric conditions (see Mather, 2015, and references therein). In recent decades, satellite and aircraft observations have identified the presence of elevated halogens at high altitudes following some (but not all) volcanic eruptions, in particular chlorine as HCl (e.g. Rose et al., 2006; Prata et al., 2007; Carn et al., 2016) and occasionally bromine as BrO (Theys et al., 2009, 2014). Co-injection of volcanic halogens alongside SO_2 into the stratosphere modifies the chemistry-climate impacts of the eruptions (Brenna et al., 2020; Ming et al., 2020; Wade et al., 2020). This occurs through feedbacks on SO_2 processing to sulfate particles (Lurton et al., 2018), depletion of ozone and other climate gases such as water-vapour and methane, with feedbacks on aerosol microphysics and transport, and thereby changing the radiative impacts (Staunton-Sykes et al., 2021). The chemistry-climate impacts of volcanic eruptions also depend on background halogen loading that is currently elevated due to historic CFC emissions. As the stratospheric halogen loading approaches pre-industrial levels in future, volcanic sulfur injections are expected to increase total column ozone whereas halogen-rich injections would deplete ozone (Klobas et al., 2017).

All these impacts of volcanic halogens depend critically on the extent of the conversion of emitted volcanic hydrogen halides into halogen radicals, a process called halogen activation. Indeed, hydrogen halides are weakly reactive and very soluble. As the result, their direct impact on atmospheric chemistry is very limited and short-lived because they are rapidly removed from the atmosphere. In contrast, halogen radicals are much more reactive chemically, in particular with respect to ozone, and less soluble. Therefore, assessing the atmospheric impacts of volcanic halogens requires a quantitative understanding of the physico-chemical plume processes driving the partitioning of volcanic halogen species, especially bromine species, between radicals and hydrogen halides. This is the primary focus of the present study. Note that only a small fraction of chlorine emissions undertakes reactive chemistry in plumes, and this small fraction is mostly activated as a result of bromine chemistry (Rüdiger et al., 2020, and references therein). As in most studies on volcanic plume halogen chemistry, fluorine and iodine are ignored. The solubility and stability of HF, the main emitted fluorine species, are such that no significant fluorine chemistry occurs within the plume (von Glasow et al., 2009). Iodine, while very reactive, is of substantially lower in-plume abundance than bromine and chlorine (Aiuppa et al., 2005).

Once emitted at high temperatures in the atmosphere, volcanic volatiles are cooled very quickly by the fast mixing of the plume with the surrounding air. Whilst some halogen radicals, as well as HO_x and NO_x, may be formed by high-temperature reactions immediately after emission from the vent (in the so-called "effective source region" see Bobrowski et al., 2007; Roberts et al., 2019, and references therein), it is the atmospheric chemistry in the cooled and expanding plume that causes a sustained halogen cycling that impacts tropospheric ozone. This halogen chemistry continues to occur as the plume disperses into the background atmosphere. This chemistry is complex and non-linear. The major bromine cycling driving bromine activation and ozone loss is shown in Figure 1. Heterogeneous processes involving acidic aerosol are the main pathway by which HBr is converted to reactive forms. The complete cycle requires photolysis reactions and therefore only occurs within the daytime. This bromine cycle is sometimes referred to as the "bromine explosion" (Wennberg, 1999; Bobrowski et al., 2007) because

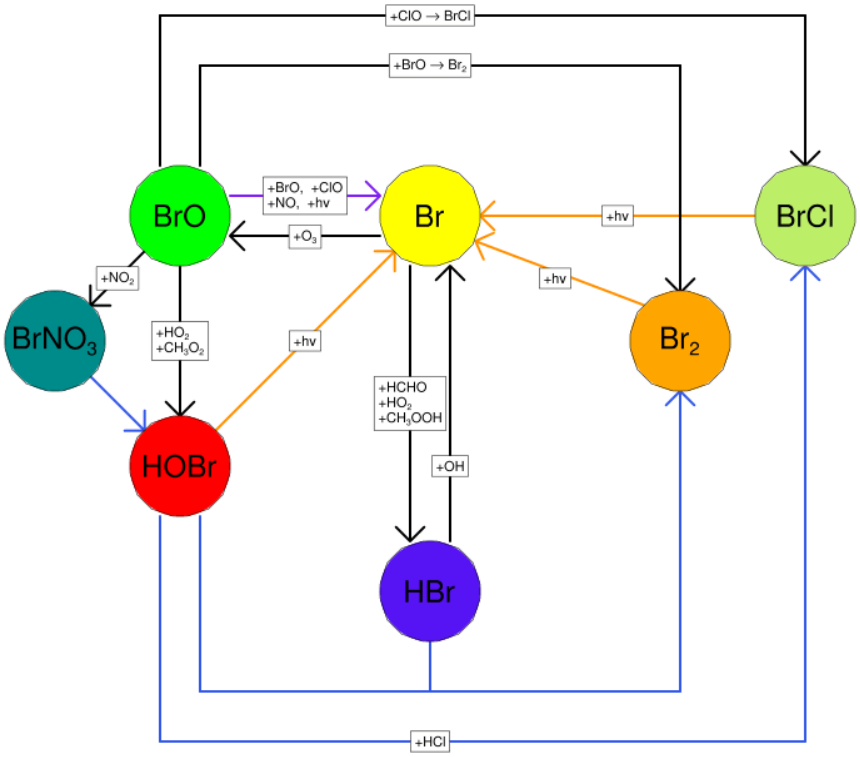

Figure 1. The major reactions of the bromine cycle. Orange lines indicate photolysis reactions, blue lines heterogeneous reactions, black lines other gas phase reactions. BrO $\longrightarrow$ Br includes one photolysis reaction and three other reactions.

of its autocatalytic nature; bromine extracted from HBr can continue to cycle and generate further reactive bromine from this source. The proportion of emitted bromine that exists as BrO impacts the in-plume BrO/SO_2 ratio. The observations of Dinger et al. (2020) show this quantity can vary with meteorological conditions. Although no equivalent "chlorine explosion" exists, heterogeneous reactions can also generate reactive chlorine radicals (via BrCl) which can react with ozone to form chlorine oxide species.

Reactive halogen chemistry in tropospheric volcanic plumes, as evidenced by enhanced BrO, has been observed for many volcanoes worldwide (Gutmann et al., 2018), with satellite observations greatly expanding the quantity and geographic scope of observations (e.g Hörmann et al., 2013).

A fast interchange exists between Br and BrO. The $Br + O_3 \longrightarrow BrO + O_2$ reaction consumes an O_3 molecule, while BrO photolysis effectively reverses this as the O radical produced quickly reacts with O_2 to form O_3. When BrO is reduced to Br via any other pathway (directly or indirectly), the net result is the loss of an O_3 molecule.

As well as depleting ozone, halogen chemistry has influences on other chemical systems, such as through reactions with NO_x and HO_x as shown in Figure 1. Volcanic halogens deplete HO_x, increasing the lifetime of SO_2 with respect to OH oxidation, and oxidation of CH_4 by Cl radicals can reduce significantly the in-plume lifetime of CH_4. Jourdain et al. (2016) modelled

both of these phenomena occurring in Ambrym plume, finding that halogens' depletive effect on HO_x to further incrased the lifetime of SO_2 with respect to oxidation by OH by 36%. Modelling by Roberts et al. (2009) indicates that volcanic halogen chemistry can result in conversion of in-plume NO_x to HNO_3.

Finally, volcanoes are also sources of mercury to the atmosphere (Pyle and Mather, 2003) mainly in the inert form Hg(0) (Witt et al., 2008; Bagnato et al., 2007). A 1D model study by von Glasow (2010) suggested that this mercury could be rapidly oxidised by halogen chemistry in a volcanic plume to more soluble forms, easily removed from the atmosphere (Seigneur and Lohman, 2008). Significant advances in understanding of the kinetics of halogen-mercury chemistry have been made in the last decade (e.g. Saiz-Lopez et al., 2018, 2019) and these are included in the modelling part of this study.

1.2 Observation and modelling studies

The current understanding of halogen chemistry within volcanic plumes is based upon a body of observations that have used a variety of techniques, coupled with numerical modelling results, most of which have used zero- or one-dimensional chemical box models.

1.2.1 Observations

There are two main methods for measuring halogens in volcanic plumes, remote sensing and in-situ sampling.

Remote sensing accounts for most observations of reactive halogens in volcanic plumes. Since the first reported detection by Bobrowski et al. (2003), bromine monoxide (BrO) has been observed within the plume of dozens of volcanoes by differential optical absorption spectroscopy (DOAS) (see Gutmann et al., 2018, for a recent catalogue of such observations) for a recent catalogue of such observations). A smaller number of measurements of in-plume ClO and OClO have also been reported. These halogen molecules have spectroscopic signatures within the ultraviolet range, meaning they can be identified from the same data that is used to monitor SO_2, including data collected from long-term DOAS monitoring networks at volcanoes (Dinger et al., 2018; Warnach et al., 2019). As well as ground and airbourne observations, BrO has been observed in the plumes of some larger volcanic eruptions by satellite-based instruments (e.g. Hörmann et al., 2013; Seo et al., 2019), though such large eruptions are the focus of a future study rather than this one.

In-situ sampling of halogens provides the most direct approach to quantify total halogen emissions: time-averaged sampling has for decades been used to quantify total volcanic halogen emission contents for F, Cl, Br and I (e.g. Aiuppa et al., 2004; Wittmer et al., 2014). Modern techniques now allow for a degree of speciation in the bromine observed through these methods (Rüdiger et al., 2017, 2020). For most reactive halogen species, these methods required samples to be collected in-situ and then subsequently analysed in-lab. Consequently, there are fewer in-situ observations of reactive halogens than by remote sensing.

As well as these direct approaches, ozone measurements can provide indirect evidence for halogen chemistry. Ozone destruction in tropospheric volcanic plumes, caused by volcanic halogen cycling, has been measured in a limited number of cases (Vance et al., 2010; Oppenheimer et al., 2010; Kelly et al., 2013; Surl et al., 2015). In ash-rich explosive eruptions, it is possible that uptake of ozone on ash particles may also contribute to some ozone loss (Maters et al., 2017). Measuring ozone in volcanic plumes in the troposphere region downwind from volcanoes is challenging and typically only achieved using instrumented air-

craft. Observations suggest a direct relation between bromine content and ozone depletion (Roberts, 2018), although this is based on only three available volcanic datasets: Mount Etna, Mount Redoubt and Kilauea. Observations at Mount Redoubt volcano suggest that ozone losses, as a ratio to SO_2, increase in magnitude with respect to the distance from the source (Kelly et al., 2013).

For the above methods, the observed halogen gas quantities or ozone depletions are often ratioed to simultaneous sulfur or SO_2 measurements. This allows for comparison between plumes of different "strengths" (i.e. density or dilution), and, for example, to trace how halogen chemistry changes as a plume disperses as it travels downwind. This use of SO_2 as a plume tracer presupposes that it has a long atmospheric lifetime relative to the timescale of the given study.

1.2.2 Numerical modelling

Another tool for studying the chemistry of volcanic plumes is numerical modelling. Most volcanic plume halogen chemistry modelling studies to date have originated from implementations of a few models, in particular MISTRA (Aiuppa et al., 2007; Bobrowski et al., 2007; von Glasow, 2010; Bobrowski et al., 2015; Surl et al., 2015) and PlumeChem (Roberts et al., 2009, 2014, 2018; Kelly et al., 2013). A more recent study by Rüdiger et al. (2020) used the CABBA/MECCA box model. These Lagrangian models are either zero- or one-dimensional and simulate the chemical evolution of the cooled plume by calculating the in-plume rates of chemical reactions and include the continual dilution of the plume with background air. Such models are found to better reproduce observations if the initial halogen emissions include a fraction of halogen radicals. This represents the radicals generated by high temperature chemistry in the effective source region.

To our best knowledge, Jourdain et al. (2016) is the only prior 3D Eulerian-type mesoscale chemistry-transport modelling study published to date dealing with halogen chemistry a tropospheric volcanic plume. Volcanic emissions and halogen chemistry were implemented into the CCATT-BRAMS model to simulate the chemistry within the plume of Ambrym volcano during an intense passive degassing episode in 2005. Their model is similar to the one used in our study. However, their gas emission flux for the Ambrym event is about six times greater than the Mount Etna passive degassing event studied here. Mechanistically, their results showed the formation of BrO, as well as ozone depletion occurring within the plume's core that impacts bromine speciation. The study also simulated in-plume depletion of HO_x and NO_x, as well as lengthening of SO_2 and methane lifetimes due to halogen chemistry. The model successfully reproduced observed BrO/SO_2 spatial patterns, however the magnitude was somewhat underestimated, and there were no measurements of ozone to provide constraints on the predictions of ozone depletion, a key feature of reactive halogen chemistry. Finally, Jourdain et al. (2016) focuses on the wider-scale impact of volcanic emissions, whereas this study focuses more on the detailed mechanisms of halogen cycling in the early plume with cross-validation against ozone and halogen radical observations.

WRF-Chem has been used in several studies to model tropospheric volcanic plumes, generally showing good agreement with observations (Stuefer et al., 2013; Burton et al., 2020; Egan et al., 2020; Rizza et al., 2020; Hirtl et al., 2019, 2020). Such studies have predominantly focused on ash and SO_2 distribution, and there have been none, to our knowledge, that incorporate halogen chemistry.

1.2.3 This study

The present study is devoted to a plume from Etna during July/August 2012, a period when this volcano was passively degassing. We present new airborne ozone and SO_2 measurements which were made during traverses of plumes at distances 7–21 km from the vents. Several other previously published plume measurements were also made around this time. Near-simultaneous near-vent (<500 m) ozone measurements and DOAS observations of BrO/SO_2 ratios around 10 km downwind were reported by Surl et al. (2015). Additionally in situ sampling of halogen emissions was undertaken that summer at the crater-rim by Wittmer et al. (2014) and further DOAS measurements were also made of Etna's plume by Gliß et al. (2015). Consequently, this period of Etna's activity may have the richest overall dataset to date for determining halogen activity in relation to ozone loss in the plume of a volcano.

The observational dataset is analysed using a 3D regional chemistry-transport model (WRF-Chem) modified with respect to its handling of volcanic emissions and with halogen chemistry added to a chemical mechanism. The goal of the modelling is to assess the ability of the 3D model to adequately reproduce the key chemistry features (ozone loss, BrO/SO_2 ratios) of the Etna plume given reasonable input parameters, such as the typical halogen emission fluxes for the volcano in a passive degassing state. We then diagnose in-plume chemical processes in the model, exploiting the fact that a model can be interrogated in far greater detail than an observational dataset. The focus is on the chemical processes in the near-downwind plume, up to 10s of km from emissions sources for plume ages of up to 10s min. As well as halogen chemistry and the associated ozone destruction, the simulated impacts of plume chemistry on the various interconnected chemical systems discussed above (HO_x, SO_2 lifetime and its oxidation to particles, methane lifetime, reactive nitrogen, and mercury chemistry) are also investigated.

2 Methods

2.1 Aircraft measurements of SO_2 and ozone in the plume

The aircraft campaign presented in this study was conducted as part of the Global Mercury Observation System project (http://gmos.eu) with the same aircraft and instrumentation discussed in Weigelt et al. (2016a) and Weigelt et al. (2016b). We refer the reader to these works for a full description of the campaign setup and instruments; in this section we highlight the most relevant aspects.

The measurements of this study were performed with a CASA 212 two-engine turboprop aircraft fitted with a specially designed gas inlet system. SO_2 was measured with a Thermo Environmental Instruments Model 43C pulsed fluorescence gas analyzer with RMS noise of 1 ppbv and precision of 1 ppbv or 1% of reading (http://www.thermo.com.cn/Resources/200802/productPDF_12267.pdf). Estimates of the interferences from H_2O and NO are reported as < 3 ppbv and < 2% of reading. Ozone was measured with a Teledyne API 400E, with RMS noise and precision < 0.5% of reading. This measurement is not subject to interference from SO_2 or H_2O as these interferences are efficiently removed by the comparison of measurements between the ambient air channel and the ozone-scrubbed reference channel (http://www.teledyne-api.com/products/oxygen-compound-instruments/t400). Mercury vapour is listed as a potential source of interference; however

mercury-detecting instruments were also active during this campaign and the level of gaseous mercury emission from the volcano was determined to be nil or low (Weigelt et al., 2016a). Both the SO_2 and ozone instruments have a temporal resolution of 10s (averaging time) and their response times are 80 seconds and < 30 seconds, respectively.

Three flights were conducted, one each on the mornings of 2012-07-30, 07-31, and 08-01, during daylight hours. These flights started and ended at Reggio Calabria Airport and attempted several transects of the plume. The flight paths are shown in Figure 2.

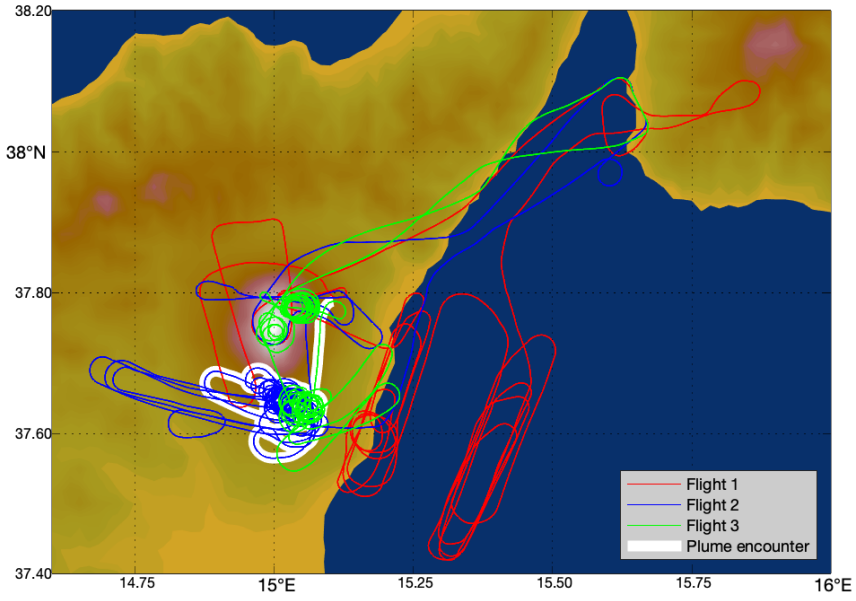

Figure 2. Flight paths of the aircraft on the three measurement days: red - 2012-07-30, blue - 2012-07-31, green - 2012-08-01. Major plume encounter locations as identified by our algorithm are highlighted in white.

Since ambient concentrations of ozone vary both spatially and temporally, rather than assessing all of the observation data together, we undertook a systematic approach to identify and isolate separate "major plume encounters" from the dataset, and evaluate separately the ozone variations within these. This approach was designed such that the majority of the variation in ozone within each major plume encounter could be ascribed to plume chemistry rather than variations in the background. Our approach also fixed a maximum range of distances from the vent that could be considered part of a single major plume encounter so as to minimise any internal variation in ozone losses within a plume encounter due to plume chemistry varying with distance from the source. Inspection of the data showed that, outside of the plume, rapid changes in altitude corresponded with substantial changes in ozone mixing ratio. In order to avoid mistaking such background ozone variation as a plume signal

we fixed a maximum range of altitudes that could be considered part of one major plume encounter. Lastly, encounters that are too short or do not reach a sufficiently high plume intensity so as to allow for an identification of signal above background variation are dismissed.

Our algorithm is therefore as follows:

- a plume encounter is considered to begin when the SO_2 measurement exceeds 10 ppbv, and ends when SO_2 drops below 10 ppbv
- If a datapoint's altitude is more than 300m higher or lower than that of any previous datapoint in the current encounter, the encounter ends and another immediately begins.
- If a datapoint's distance from the source is more than 5 km greater or smaller than that of any previous datapoint in the current encounter, the encounter ends and another immediately begins.
- if a plume encounter has maximum SO_2 less than 100 ppbv, or lasts for less than 2 minutes, it is considered a "minor plume encounter" and is discarded

This process is presented in full as a flowchart in Figure S1.

2.2 Modelling

We use version 4.1.5 of WRF-Chem (Grell et al., 2005) which is a fully coupled three-dimensional regional model for atmospheric physics, meteorology and chemistry, including cloud and aerosol radiative feedback processes. We have made several modifications to the code, in particular volcanic gas emissions and chlorine/bromine/mercury chemistry. We name this new model "WRF-Chem Volcano" (WCV). Our WCV developments build on the WRF-Chem version developed by the Roland von Glasow group at the University of East Anglia (Surl, 2016) and our WCV developments were made with reference to the model code of Badia et al. (2019), another development on the University of East Anglia version with a focus on marine chemistry.

2.2.1 Mechanism

WCV extends the CBMZ-MOSIAC chemistry scheme with 8 aerosol size bins (Zaveri and Peters, 1999; Zaveri et al., 2008) to include bromine, chlorine, and mercury chemical mechanisms with gas-phase, photolytic, and heterogeneous reactions involving the following species: HBr, Br, BrO, HOBr, $BrNO_3$ (a.k.a. $BrONO_2$), Br_2, HCl, Cl, ClO, OClO, HOCl, $ClNO_3$, Cl_2, BrCl, Hg, HgBr, HgCl, $HgBr_2$, $HgCl_2$, and HgBrCl. We exclude $BrNO_2$ as previous studies have found it to be a negligible component (Roberts et al., 2014; Rüdiger et al., 2020). These species are also incorporated into the dry- and wet-deposition schemes and the FastJ photolysis scheme (Wild et al., 2000). The rates of heterogeneous reactions involving HOBr, $BrNO_3$, and $ClNO_3$ on volcanic aerosols are calculated on-line accounting for the wet surface area of aerosol and gas-phase diffusion limitations as described by Marelle et al. (in review). The products of HOBr reactive uptake are partitioned between Br_2 and BrCl (i.e. net overall reaction with HBr or HCl) by a parameterization that assumes fast aqueous-phase equilibria between Br_2,

Br_2Cl^-, and BrCl as described by Jourdain et al. (2016). Reactions added to the scheme are listed in the supplement (Tables S1, S2, S4) along with their rate equations and references for these. Parameters controlling the heterogenous reactions are tabulated in Table S3.

The only SO_2 oxidation pathway included in CBMZ-MOSAIC is oxidation by OH, and we did not add any further pathways. Galeazzo et al. (2018) discusses other pathways could potentially occur in the aqueous phase in volcanic plumes: oxidation by O_{3aq}, oxidation by H_2O_2, and transition-metal-catalysed oxidation by O_2.

Our volcanic emissions pre-processor, a modified version of the the PREP-CHEM-SRC utility (Freitas et al., 2011), provides as inputs to the model fluxes of sulfur, bromine, chlorine, and mercury species as well as an 'at-source' sulfate particle flux, and fluxes of radicals resulting from high-temperature chemistry within the vent (e.g. OH, NO). This emission is time-invariant, and is into a single grid cell of the model (c.f. the more spatially and temporally sophisticated pre-processor of Hirtl et al. (2020)).

We have also introduced artificial tracer species to WCV that do not influence the chemistry but are useful for analysis. *tracer1* is a wholly inert species that is emitted with the same flux rate as SO_2. *tracer1* is used to compute mean (weighted average) in-plume values of parameters — here an 'in-plume average' of a value (e.g. of ozone mixing ratio) refers to the average of this value across all grid boxes where *tracer1* exceeds 3 ppbv, weighted by the *tracer1* content of the boxes.

tracer2 is similar to *tracer1* but undergoes a first-order exponential decay with specified rate. The ratio of *tracer1* and *tracer2* can therefore be used to derive the mean time-since-emission of any part of the plume. This approach allows us to accurately calculate plume-age in any model grid cell and enables us to monitor how plume parameters (e.g. ozone mixing ratio, BrO/SO_2 ratio) vary with the plume time evolution since emission.

We have also added to the model output monitoring of several chemistry diagnostics, such as rates of relevant reactions, in order to carry out species' chemical budgets and therefore facilitate the analysis of the underlying halogen and ozone-destructive chemistry.

2.2.2 Model settings

The total area modelled, at 30 km horizontal resolution, is depicted in Figure 3a. Also shown are the extents of the progressively nested domains, each modelled with grid dimension three times smaller than their parent. These domains are two-way nested in exchanging meteorological, chemical, and physical information between them. Here we focus on the near-downwind plume processing (up to about 90 minutes). Therefore all the figures and results presented in this study are from the *d04* nest (Figure 3b) which models an 88 km $\times$ 134 km area around the east coast of Sicily with a horizontal spatial resolution of 1.1 km. The model has 50 vertical layers, extending up to 50 hPa.

The model was initialised at 2012-07-29 00:00 and ran for four days, therefore covering all of the days of the aircraft measurements. The first 24 hours are considered spin-up, results are presented from > 24 hours onwards.

The volcano was considered to be a point source of gas and aerosol, emitting at a constant flux rate throughout the simulation period. Although Mount Etna has several active vents (North-east Crater, Voragine, South-East Crater) at the volcano summit, the maximum horizontal resolution of the model is not sufficient to distinguish these. Emissions are released into a single grid

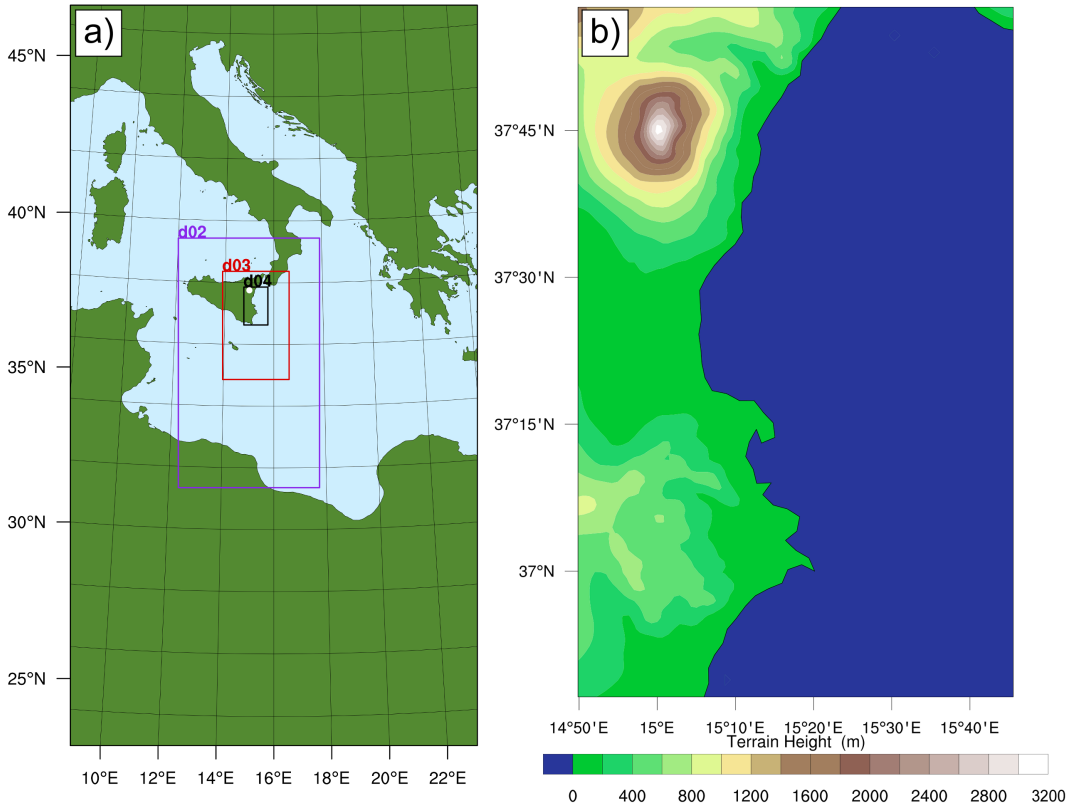

Figure 3. a) The WCV model area. *d02*, *d03*, and *d04* are progressively nested domains with two-way nesting. b) Terrain elevation in *d04*

cell at 37.751°N, 14.995°S, and 3300 mASL, the location of the summit peak of Etna. This altitude does not correspond to the lowest model level at this location but rather a few levels above it because, even at the maximum model resolution, the sub-grid topography of Etna volcano is smoothed out in the model grid box. For example, at the 1.1 km resolution, the ground altitude of the Etna grid box is 3088 m. The lower the model resolution is, the more potent the smoothing of sub-grid terrain features is, and hence the greater this discrepancy is.

Modelled emissions of SO_2 were set to 40 kg s^{-1}. This flux was estimated by adjusting initial estimates according to comparisons between outputs from preliminary runs and observed SO_2 mixing ratios. A 40 kg s^{-1} flux results in SO_2 mixing ratios within the centre of the modelled plume being similar to the maximum SO_2 mixing ratios observed from the aircraft at the same distance from the source. We assume these observed maxima correspond to transects which cross or come close to the core of the plume. 40 kg s^{-1} also falls mid-way within the normal range of measured SO_2 fluxes (41 ± 30) kg s^{-1} for Etna's activity during non-eruptive (passive degassing) periods (Salerno et al., 2009). A volcanic H_2O flux is set to be 15 times greater (in terms of number of molecules) than the SO_2 flux following Aiuppa et al. (2008). Being effectively inert chemically, CO_2 and its emissions are ignored in the model.

Mount Etna's plume also contains sulfate-rich particles whose presence in the young plume at the volcano summit (Martin et al., 2012; Roberts et al., 2018) indicates they are formed early on, possibly in the vent, well below the grid resolution of the model. These 'at-source' aerosols are treated as primary aerosols. They are included in the model by setting a volcanic aerosol emission flux which is derived from the reported near-summit sulfate/SO_2 mass ratio of 0.03 (Roberts et al., 2018). All of this aerosol is taken to be sulfate with a size distribution into the 8 MOSAIC size bins following that of Roberts et al. (2018), with an extrapolation made for the smallest bins. During the in-situ measurements of Surl et al. (2015) made on the 30th June and 1st August the plume was observed to be ash-free. Therefore no ash was included in this modelling.

Chlorine and bromine emission fluxes are specified based on the observed summit chlorine-to-bromine ratio and HCl-to-SO_2 ratio and the SO_2 flux specified above. We rely on a comprehensive compositional analysis undertaken between June 2010-June 2012 by Wittmer et al. (2014). The chlorine-to-bromine ratio was fixed to 300 by mass (683 by mole), which is an average calculated for the Bocca Nova and North-East craters' compositions reported by Wittmer et al. (2014). The HCl-to-SO_2 ratio was set to 0.4 mol/mol which is about mid-way in the range of ratios (0.29 to 0.56) for these craters.

As stated in the introduction, volcanic gases are believed to react at high temperatures immediately following their release in the vent and into the atmosphere, generating radicals, notably HO_x and some halogen radicals. These radicals — as well as the primary aerosols —- subsequently initiate the onset of the bromine cycling in the cooled plume (Figure 1). A representation of the high-temperature radicals is therefore needed for the WCV volcanic input. Thermodynamic models have been used previously to represent this high-temperature "effective source region" (Bobrowski et al., 2007) but their assumption of chemical equilibrium is not considered reliable, whereas recently developed kinetic models do not yet include halogens (see Roberts et al., 2019). Here we choose a simpler approach by, in the *main* run, partitioning the bromine emission flux into hydrogen halide and radicals, with 75% of bromine emitted as HBr and 25% as Br radicals, and by including a HO_x emission. This bromine partitioning follows previous thermodynamic modeling estimates (Roberts et al., 2014). Emissions of volcanic HO_x are highly uncertain, there exist order-of-magnitude differences between kinetic and thermodynamic model predictions, and in the speciation between OH and HO_2 (Roberts et al., 2019). Here, we define the volcanic HO_x emission by setting a OH/SO_2 molar ratio of 0.001 (between reported thermodynamic and kinetic model ranges). The immediate reaction of OH with SO_2 in WCV will generate HO_2 and some additional sulfate. Whilst all volcanic chlorine is emitted as HCl in the model, the reaction with volcanic OH will also quickly generate some Cl radicals.

Although there are open questions regarding the kinetics of high-temperature NO generation in the first few seconds of plume evolution (Martin et al., 2012), we chose to include these emissions to assess its possible effect. We use an NO/SO_2 molar emission ratio of 4.5×10^{-4}, which is of the order typically produced by high temperature thermodynamic modelling of the early plume-air mix (c.f. 6.6×10^{-4} used in Roberts et al. (2014)).

Although the aircraft campaign did not find a detectable mercury signal for the plume (Weigelt et al., 2016a), we include a small mercury emission so as to investigate this mechanism. We use a general volcanic emission ratio of 7.8×10^{-6} mol Hg per mol SO_2 from Bagnato et al. (2014), a quantity too small to significantly interfere with other chemical systems. All of this mercury is emitted as Hg(0).

Species	Flux / s^{-1}	Ratio to SO_2	
		mass	molar
SO_2	40 kg	1	1
Br	7.6 g	1.89×10^{-4}	1.5×10^{-4}
HBr	23 g	5.66×10^{-4}	4.5×10^{-4}
HCl	9.0 kg	0.226	0.4
OH	11 g	2.7×10^{-4}	1.0×10^{-3}
NO	8.4 g	2.1×10^{-4}	4.5×10^{-4}
H_2O	169 kg	4.2	15
Hg	0.9 g	2.4×10^{-5}	7.8×10^{-6}
Aerosol	1.2 kg	0.03	0.02

Table 1. Volcanic emission fluxes in the *main* model run

We use external data for model forcing at the boundaries of the outermost domain and for the initial conditions of the model. Meteorological information is sourced from the NCEP FNL Operational Model Global Tropospheric Analyses (National Centers for Environmental Prediction et al., 2000). Chemical information is sourced from CAM-CHEM (Buchholz et al., 2019; Emmons et al., 2020) and applied using the MOZBC utility. Since mercury, bromine and chlorine species other than HCl were absent from this CAM-CHEM data, we set their initial and boundary values to zero.

As well as the *main* model run detailed above, several other model runs were made with varying emissions (Table 2). These include a model run with no volcanic emissions (*novolc*). Differences between *novolc* and the other runs are used to quantify volcanic impacts. Sensitivity runs were identical to the main run except for the perturbations to the volcanic emissions listed in Table 2. The *noHighT* run excludes all species expected to be generated in the high temperature volatile-air mix of the first few seconds after volcanic emission, and therefore includes only H_2O, SO_2, HCl, and HBr (all bromine as HBr) as well as primary sulfate.

3 Aircraft observations quantifying ozone destruction in the plume

The encounter-finding algorithm described in Section 2.1 yields 19 major plume encounters, 11 on the 31st July and 8 on the 1st August 2012. Only minor plume encounters occurred on the 30th July. The locations of these major encounters are highlighted in Figure 2. Plots of O_3 vs. SO_2 for these encounters are shown in Figure 4 for the 31st July and Figure 5 for the 1st August. These data are also summarised in Table 5.

For the majority of encounters, there is a clear anti-correlation between O_3 and SO_2, with linear fits yielding negative gradients for most encounters, which is consistent with continuous O_3 destruction during the plume evolution. In several plots, the anti-correlation between SO_2 and O_3 variations is evident from aligned data points corresponding to consecutive observations. All encounters span ranges of several km, in which the background O_3 is liable to vary. We believe this is a

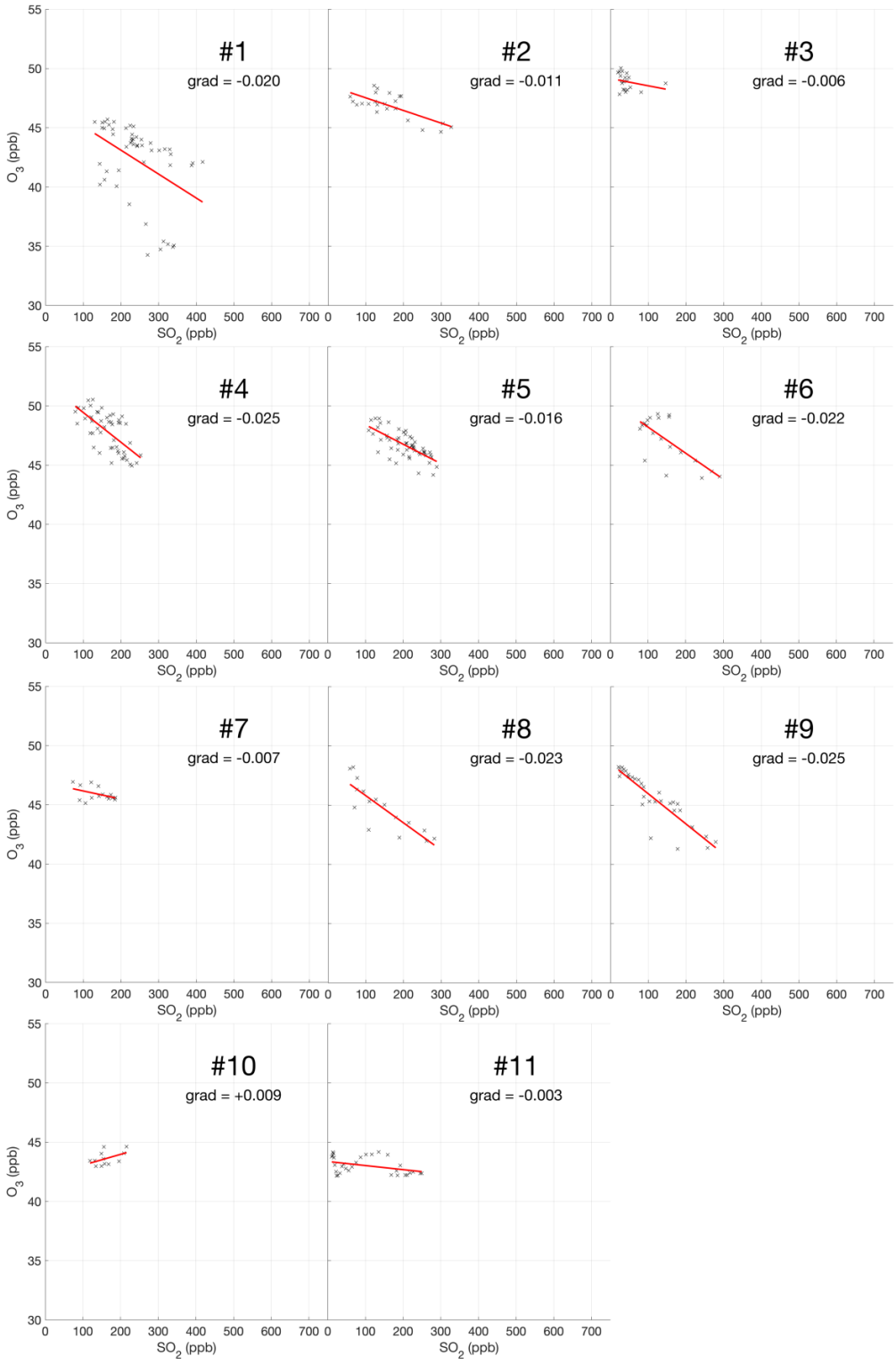

Figure 4. Measurements of SO_2 and O_3 mixing ratios for the 11 major plume encounters on 2012-07-31.

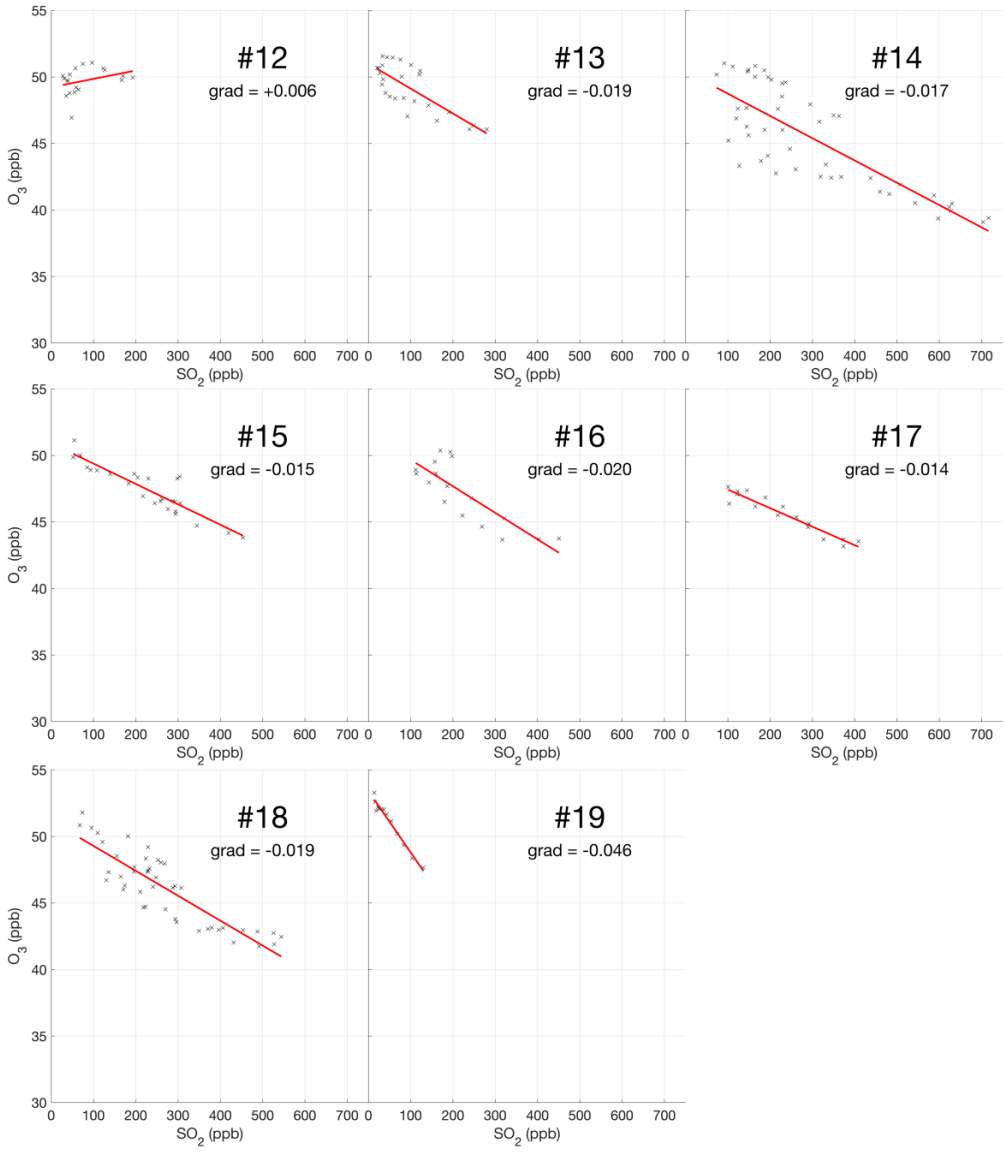

Figure 5. Measurements of SO_2 and O_3 mixing ratios for the 8 major plume encounters on 2012-08-01.

Run	Relative volcanic emission rate								HBr:Br
	SO_2	H_2O	aerosol	Br_{total}	HCl	OH	NO	Hg	
main	1	1	1	1	1	1	1	1	75:25
novolc	0	0	0	0	0	0	0	0	N/A
noHighT	1	1	1	1	1	0	0	1	100:0
mag33	0.33	0.33	0.33	0.33	0.33	0.33	0.33	0.33	75:25
mag150	1.5	1.5	1.5	1.5	1.5	1.5	1.5	1.5	75:25
hal00	1	1	1	0	0	1	1	1	N/A
hal33	1	1	1	0.33	0.33	1	1	1	75:25
hal150	1	1	1	1.5	1.5	1	1	1	75:25
oth33	0.33	0.33	0.33	1	1	0.33	0.33	0.33	75:25
oth150	1.5	1.5	1.5	1	1	1.5	1.5	1.5	75:25
br50_50	1	1	1	1	1	1	1	1	50:50
br90_10	1	1	1	1	1	1	1	1	90:10
br95_5	1	1	1	1	1	1	1	1	95:5
br100_0	1	1	1	1	1	1	1	1	100:0
NO_00	1	1	1	1	1	1	0	1	75:25
OH_25	1	1	1	1	1	0.25	0	1	100:0
OH_10	1	1	1	1	1	0.1	0	1	100:0

Table 2. Volcanic emission rates of species in the model runs of this study; relative to those of *main*, and speciation of bromine at emission.

significant secondary source of variations in O_3 in these encounters. Mixing of the plume with external air with varying levels of O_3 would generate random fluctuations in the data and alter the O_3/SO_2 gradient and its correlation with the plume density. This is the most likely cause for the apparent curvatures when plotting some series of consecutive observations. In the case of encounters 10 and 12, this secondary source of variation obscures the primary effect producing slightly positive gradients.

These observational data show that ozone is depleted within the plume, and this depletion is proportional to the intensity of the plume as quantified by SO_2 measurements.

Weighting by the duration of each encounter and their R^2 values, the average O_3 vs. SO_2 gradient for the plume encounters is -0.018 molec molec^{-1}, and the average distance from the source is 14 km. Assuming that ozone destruction is a continuous process, and that, at distance zero, ozone destruction is zero, these value can be used to quantify the rate of ozone destruction as a ratio of SO_2 per km traveled; the resulting value is 0.0015 molec molec^{-1} km^{-1}. This could be converted to a destruction-per-second value by dividing by wind speed. No wind speed data was collected during the flights, so to do this we inspect the meteorological output from the model, which yields for both days a wind speed for the plume of approximately 9 m s^{-1} at the time of the flights. Using this value yields a rate with respect to time of -1.3×10^{-5} molec molec^{-1} s^{-1}. Interestingly, this rate is very close to a value of -1.0×10^{-5} molec molec^{-1} s^{-1} derived from in-situ measurements made within 500 m of the

vents on 27–30 July 2012 (Surl et al., 2015), supporting the theory of a continuous process beginning from no ozone depletion at source.

We note that an analysis to evaluate the trend in ozone depletion with respect to distance within the dataset yielded a null result: ozone depletion to SO_2 ratios were calculated for each in-encounter datapoint by using the y-axis intersect of each plume encounter as an estimate for background ozone for all datapoints within that encounter. The output from this analysis across the whole dataset was too noisy to discern an overall trend.

The observed depletion of ozone in Mount Etna plume is consistent with ozone-destructive halogen chemistry in volcanic plumes (Gutmann et al., 2018, and references therein). Halogens were not measured by the aircraft but ground-based remote sensing confirms the presence of volcanic BrO in the plume during July-August 2012 (Surl et al., 2015).

The following section presents the results of 3D high-resolution WCV model simulations, focusing on the ozone-destructive halogen chemistry in Mount Etna plume during the 2012 aircraft campaign. The model is used to quantify the ozone depletion and attribute it to specific halogen reactions, and to investigate additional impacts of volcanic plume halogen chemistry on atmospheric HO_x, NO_{xy} and mercury. Observational data and the model outputs are compared in Section 4.4.2, where parameters relating to the observed plume encounters and the linear regressions applied to them are also tabulated (Table 5) along with model data.

4 Modelling of the atmospheric chemistry of Mount Etna's plume

All results discussed in this section are from the *main* model run unless otherwise stated. We have paid particular attention to the results relating to 0800 UTC on each of 2012-07-30, 07-31, and 2012-08-01 as the aircraft was sampling the plume at approximately this time.

In several cases we use plume age as a variable. This is determined from the tracers, as discussed in the Methods.

4.1 SO_2, aerosol, and HO_x

Before investigating the halogen chemistry of the volcano plume, we first look at SO_2. The volcano emits 40 kg of SO_2 per second throughout the simulation. This produces a plume that travels downwind, dispersing (i.e. diluting) during transport – SO_2 mixing ratios decrease with time and distance from the source (Figures 6, 14). The CBMZ-MOSAIC reaction scheme includes gas-phase oxidation of SO_2 by OH, generating secondary sulfate aerosol. We note that the model does not contain other potentially significant SO_2 loss mechanisms which occur in the liquid phase (Galeazzo et al., 2018). The importance of these liquid-phase pathways is likely diminished in a passive degassing plume that does not form a water cloud, which is the case studied here. Nevertheless, the results of this section concerning SO_2 oxidation should be interpreted with caution.

For plumes aged less than an hour, the modelled mixing ratios of SO_2 and *tracer1* in the plume are nearly identical (Figure 6), indicating that SO_2 losses via OH oxidation in this period are negligible. This gives confidence to the use of SO_2 as a plume tracer.

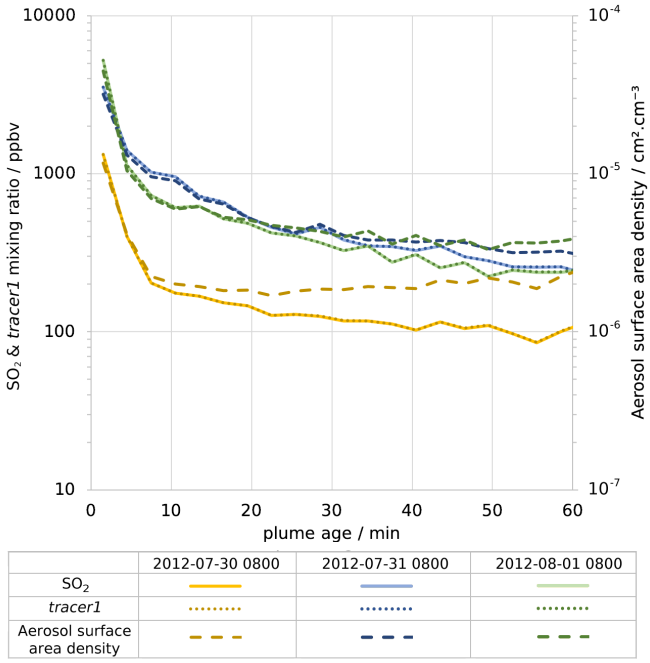

Figure 6. Modelled average in-plume mixing ratios of, on left axis, SO_2 (solid lines) and *tracer1* (dotted lines) and, on right axis, density of aerosol surface area (dashed lines). Values are plotted against plume age for 0800 UTC for each of 2012-07-30 (yellow), 2012-07-31 (blue), and 2012-08-01 (green). Note that both y-axes are logarithmic.

The average mixing ratio of SO_2 in the plume of the 30th July is, for plume ages less than an hour, typically around a third of the equivalent parts of the plume on the other two days (Figure 6), although the declining trend of SO_2 mixing ratios with age is similar. This difference is due to the fact that the wind speed on the 30th is much higher than on the other two days: the average wind speeds in the < 60 min old plume at 0800 UTC are 19, 9, and 9 m s^{-1} for the 30th July, 31st July, and 1st August respectively. Therefore, volcanic emissions are released into a greater volume of air on the 30th, yielding lower concentrations of volcanic volatiles and volcanic aerosol within the plume. As a consequence, the aerosol surface area density within the plume on the 30th is lower, though secondary aerosol production reduces this difference as the plume evolves (Figure 6).

The volcano is a direct source of aerosols, with a flux of 1.2 kg of sulfate per second in the model. This is important for the halogen chemistry as it provides a surface for HOBr uptake, enabling heterogeneous reactions. Figure 7a shows that, shortly after emission, the in-plume ratio of sulfate to SO_2 is slightly above the emission ratio of 0.03 because of the early oxidation of SO_2 by volcanogenic OH (released in the emission grid box to account for high-temperature radical production) which produces additional sulfate. This ratio continues to increase with plume age due to ambient temperature oxidation by OH mixing in from background air.

There are similar trends for the aerosol surface area-to-SO_2 ratio (Figure 7b), the increase in this ratio shows that the secondary aerosol formation notably increases the surface area available for HOBr uptake. When considered in absolute terms,

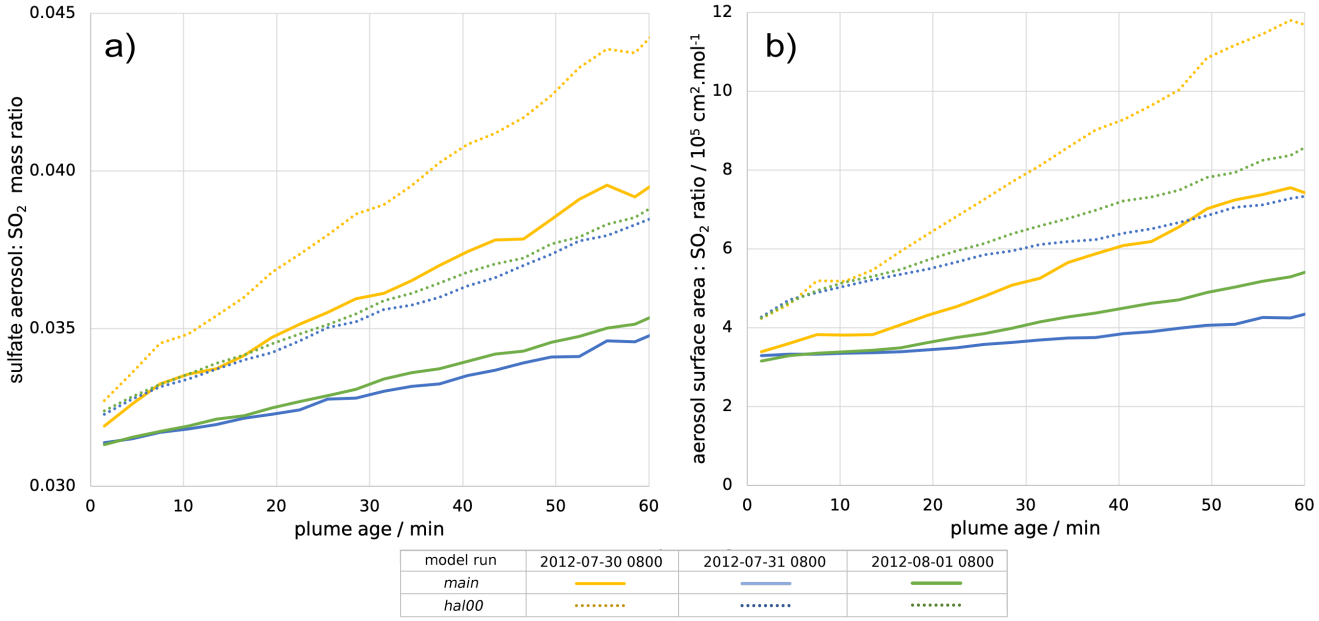

Figure 7. a) Mass ratio of sulfate aerosol to SO_2 within the plume, and b) Ratio of the total in-plume aerosol surface area to SO_2 concentration, both plotted against plume age for 0800 UTC for each of 2012-07-30 (yellow), 2012-07-31 (blue), and 2012-08-01 (green). Solid lines are for the *main* model run, dotted lines are for the *hal00* run, see Table 2

this secondary aerosol formation partly offsets the decline in aerosol surface area density caused by plume dispersion. This can be seen on Figure 6 where the aerosol surface area density declines at a slower rate than SO_2 mixing ratio. For the 30th the aerosol surface area density is approximately constant after 10 minutes, indicating that the secondary formation compensates for the dispersion in this regard.

Although the oxidation of SO_2 is not significant over these time scales with regard to SO_2 mixing ratios, the oxidation that does occur is significant for in-plume aerosol and HO_x levels. There is a substantial depletion of OH within the plume, and a moderate depletion of HO_2 (Figure 8) — for plume aged around 30 minutes OH and HO_2 levels are depleted by around 85% and 40% respectively (Table 3). This occurs despite the modelled volcano being a source of OH — this emitted OH is consumed very quickly. This result is consistent with the model findings for the Ambrym plume of Jourdain et al. (2016), who modelled total OH loss occurring in the core of that plume.

Volcanic halogens and SO_2 compete for reaction with the available OH in the model. The abundance of SO_2 in the plume results in substantial conversion of OH to HO_2 via the SO_2 + OH reaction. This starts a chain of reactions with short-lived intermediate species that is simplified to a single $SO_2 + OH \longrightarrow HO_2 + H_2SO_4$ reaction in the model (Bekki, 1995; Galeazzo et al., 2018). Volcanic HCl is also abundant and removes OH by the $HCl + OH \longrightarrow H_2O + Cl$ reaction. A similar reaction of HBr also occurs, but HBr is much less abundant. HO_2 is consumed as part of the bromine cycle in the $BrO + HO_2 \longrightarrow HOBr$ reaction.

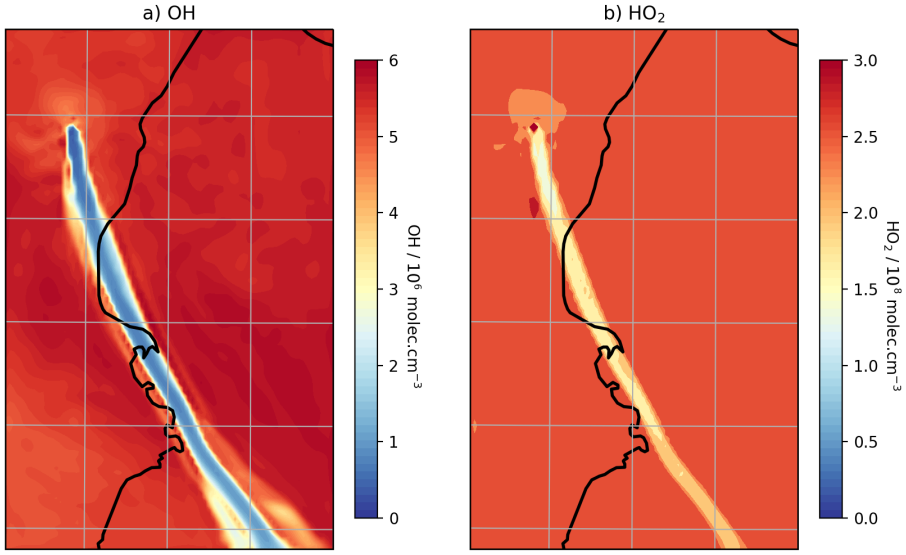

Figure 8. Modelled mixing ratios of a) OH and b) HO_2 at 3300mASL at 0800 UTC on 2012-08-01.

model run	HO_2 / molec cm^{-3}	OH / molec cm^{-3}	SO_2 lifetime / h
novolc	2.6×10^8	5.8×10^6	53
hal00	4.6×10^8	1.4×10^6	240
main	1.6×10^8	0.9×10^6	390

Table 3. In-plume concentrations of HO_2 and OH and instantaneous lifetime of SO_2 with respect to oxidation by OH for plume aged 30 ± 5 min at 0800 UTC on 2012-08-01 for three model runs. Figures for the *novolc* use the same grid cell weighting as the *main* model run.

Table 3 compares the weighted average mixing ratios of HO_x species and the instantaneous SO_2 lifetime within the plume for the *main* run, the halogen-free *hal00* run, and the equivalent model cells in the plume-free *novolc* run. Comparing these, it can be seen that the non-halogen components of the plume are sufficient to cause substantial OH depletion, whilst halogens are the cause of HO_2 depletion — the *hal00* plume actually has greater HO_2 compared to the *novolc* case.

Compared to the *novolc* case, the instantaneous lifetime of SO_2 with respect to oxidation by OH is substantially increased in the halogen free plume (*hal00*) due to the reduced OH concentrations which are caused by high SO_2 levels. The addition of halogens to the *hal00* scenario, i.e. moving to the *main* case run, further suppresses OH and hence reduces even more SO_2 oxidaion, further increasing its lifetime. For the plume part tabulated in Table 3, the instantaneous lifetimes of SO_2 for the *hal00* and *main* model runs are, respectively, 4.5 and 7.4 times that for the *hal00* run. Slower SO_2 oxidation results in slower secondary aerosol production, as seen in terms of both mass and surface area (Figure 7). This result for a tropospheric volcanic plume mirrors findings from a recent study of a stratospheric volcanic cloud (Lurton et al., 2018).

Whilst a detailed analysis of the aerosol microphysics and climate impacts of volcanic aerosols lies beyond the scope of this study, our simulations show substantial differences in the plume sulfate particle surface area density for WCV model simulations with and without volcanic halogen emissions. As plume halogen chemistry exerts an important influence on the oxidation rate of volcanic SO_2 and associated formation of secondary aerosol, our results suggest that models simulating chemistry-climate impacts of volcanic sulfur should not ignore the chemistry of volcanic halogens.

4.2 Bromine speciation and BrO/SO_2 ratio

In the *main* model run, bromine is emitted from the volcano as HBr and Br in a 3:1 ratio. During daylight this is rapidly converted to other forms, including BrO. Figure 9 shows how the forms which this bromine takes vary between plume of

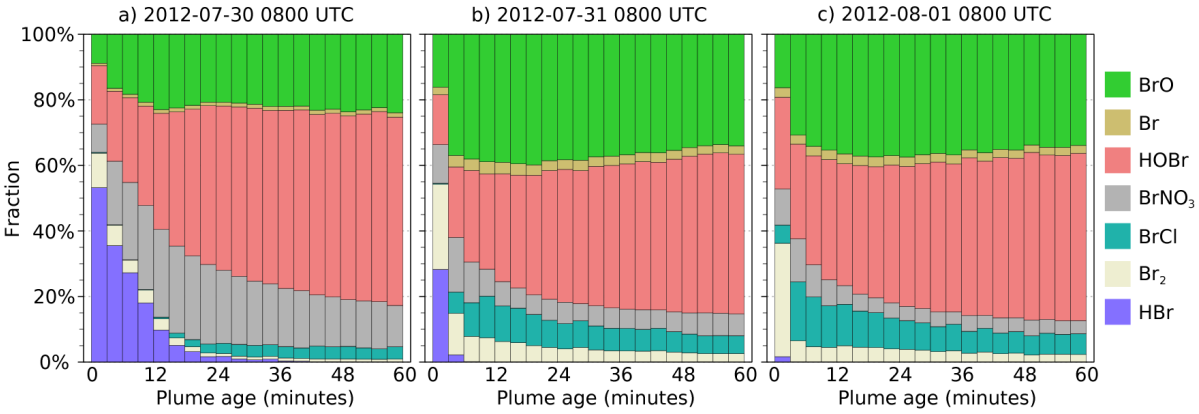

Figure 9. Differentiation of bromine between species for plume of different ages ranging from 0–60 minutes, for plume at 08:00 UTC on a) 2012-07-30, a) 2012-07-31, c) 2012-08-01

different ages at 08:00 UTC on the 30th, 31st and 1st. In this model output, HOBr becomes the dominant form of bromine within the plume, followed by BrO. The fraction as BrO increases over approximately the first 20 minutes before reaching an approximately stable fraction. A significant amount of Br_2 is formed shortly after emission but this fraction declines, with BrCl being the larger fraction of the two halogen dimers. A significant reservoir of $BrNO_3$ that forms shortly after emission declines slowly over time.

There are significant quantitative differences between the bromine evolution on these three days, although the trends are similar. These differences occur despite the emission parameters being the same for all days. Compared to the other two days, HBr and $BrNO_3$ persist in the plume for much longer on the 30th July. The balance between HOBr and BrO is more greatly tilted towards the former on that day because the in-plume aerosol surface area density is lower on the 30th (see Section 4.1 and Figure 6), reducing the rate of heterogeneous reactions that consume HBr, $BrNO_3$, and HOBr. Additionally, the reaction of BrO with background HO_2 to form HOBr is suppressed under more concentrated plume conditions due to the depletion of HO_2 discussed in Section 4.1.

Although the bromine speciation appears roughly stable after approximately 30 minutes of evolution, this does not indicate that no further chemistry is occurring, bromine is instead continually cycled between forms. This is shown in Figure S3 which depicts the rates of transfers between bromine species. "Stability" indicates a state where the chemical formation and loss of each species is approximately balanced, i.e. a steady state.

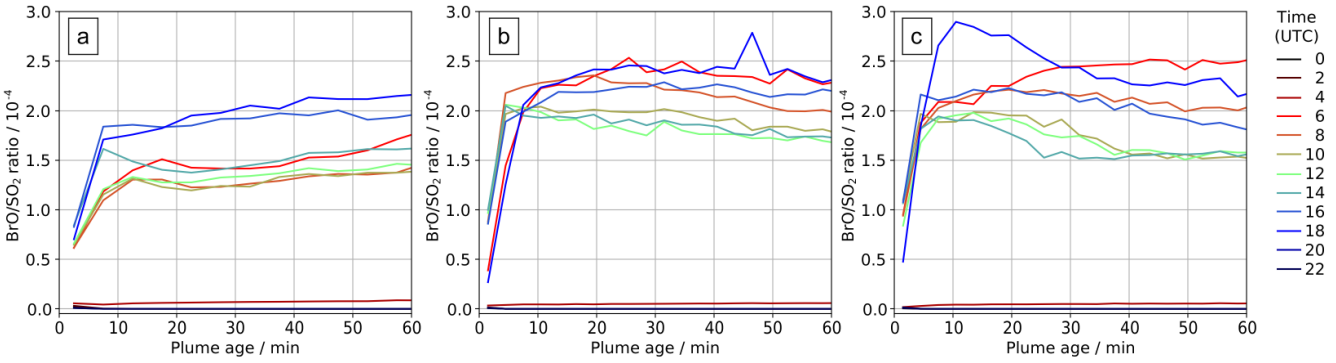

Figure 10. In-plume average BrO/SO_2 ratios for plume of different ages ranging from 0–60 minutes, at several times on a) 2012-07-30, b) 2012-07-31, c) 2012-08-01

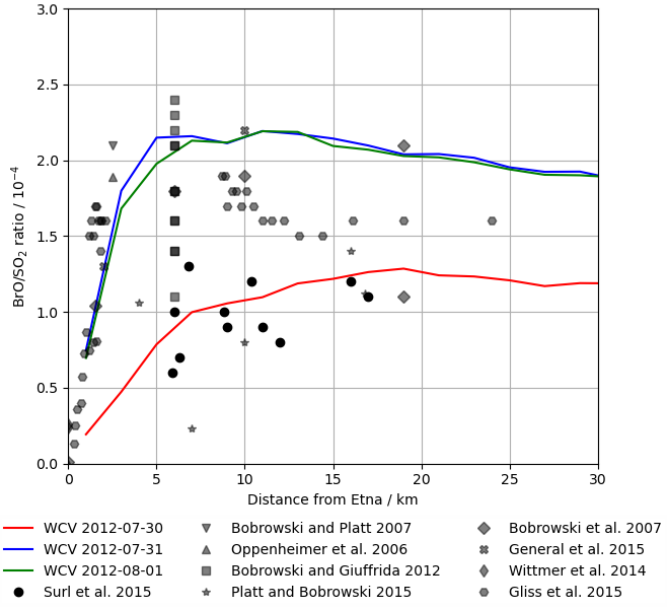

Figure 11. Modelled BrO/SO_2 ratio at 1200 UTC on 2012-07-30, 2012-07-31, and 2012-07-31 (lines), and observed BrO/SO_2 ratios in Etna plume from several studies (markers), plotted against distance from the volcano. We caution that these observations, taken on several days with varying wind speeds, should not be interpreted as representing temporal evolution.

The ratio of total bromine and SO_2 is mostly invariant in the plume, therefore the variations in bromine speciation with plume age yield variations of in-plume BrO/SO_2 ratios. There is an initial rise in BrO/SO_2, followed by a small decrease in some cases, and then a plateau. This pattern varies with time of day, as shown in Figure 10. Sunrise is shortly after 04 UTC and sunset shortly after 18 UTC. Negligible BrO is formed in the model plume at night. We find on all three days that BrO/SO_2 ratios are generally greater in the morning and evening than during the middle of the day. This occurs because BrO is more rapidly converted to HOBr in the middle of the day when atmospheric HO_2 is at a maximum. Although moderate in magnitude, this phenomenon may be significant when comparing spectroscopic columns at different times, including datasets from low-earth orbit satellites with overpasses at different local times.

Our model study identifies how variations in time-of-day and plume intensity (which is controlled by wind speed in this constant-emission case) impact BrO/SO_2. These may present additional complications for the interpretation of BrO/SO_2 ratios observed in passively degassing volcanic plumes. Variations of BrO/SO_2 are often evaluated with respect to distance from a volcano. We note that the wind speed has a "double effect". First, faster winds give the impression that the chemistry evolves more slowly as a function of distance downwind because the plume moves further from the source in a given time. Second, all other factors being equal, the along-plume dilution is expected to be stronger at higher wind velocities, affecting the in-plume chemistry and bromine speciation through the influx of background ozone-rich air.

4.2.1 Comparison to observed BrO/SO_2 ratios

No measurements of in-plume BrO/SO_2 column ratio were made as part of this study. However the DOAS-measured BrO/SO_2 columns reported in Surl et al. (2015) span from 2012-07-24 to 2012-08-02 which includes our time period. These observations, were made between 5 and 17 km from the volcano at approximately the middle of the day. Figure 11 plots these observations alongside the modelling data for 12 UTC each day. These observed ratios, ranging from 0.6 – 1.3×10^{-4}, are at about half of the equivalent modelled ratios for the 31st July and the 1st August, and are comparable, although still slightly lower on average, to those modelled for the 30th, where the initial rise in BrO/SO_2 ratios occurs over the first 15-20 km.

Although not simultaneous with the time span of this study, BrO/SO_2 measurements made close to the vents the following month (2012-09-11 – 2012-09-26) reported by Gliß et al. (2015) are also a relevant comparison. BrO/SO_2 ratios were found rising rapidly with travel time from the vent, reaching about 1.3×10^{-4} at about 150 seconds travel time and then remaining at this level. This rapid rise, and higher ratio, has better agreement with the observations of the 31st and 1st.

More generally, the shape of the modelled BrO/SO_2 versus distance/time trend seen in Figures 10, 11, and 13a — of an initial rise followed by a steady value — is in agreement with the general trend observed for Etna (Figure 11) and other volcanoes (Gutmann et al., 2018).

4.2.2 Importance of high-temperature volcanic products

In the *main* model run, Br and OH radicals are included in the model volcano emission — representing their high-temperature generation in the “effective source region” (see 2.2.2). The importance of these in the autocatalytic processes of the bromine

explosion can be seen by inspecting the output from runs in which the emission strengths of different radicals vary (see Table 2). Figure 12 compares in-plume BrO/SO_2 ratios for the *main* case with the results from several other such runs.

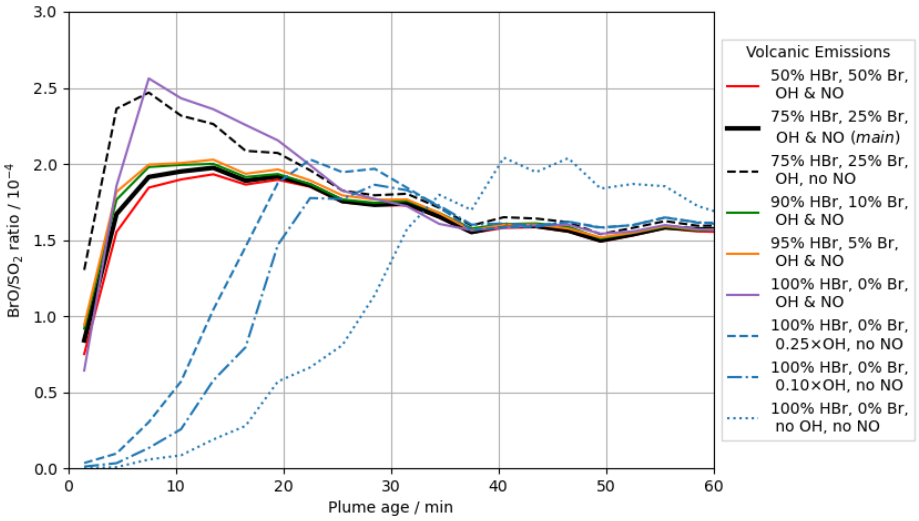

Figure 12. Modelled in-plume BrO/SO_2 ratio at 1200 UTC on 2012-08-01 versus plume age, for the following model runs: *br50_50* (red, solid), *main* (black, solid), *NO_00* (black, dashed), *br90_10* (green, solid), *br95_5* (orange, solid), *br100_0* (purple, solid), *OH_25* (blue, dashed), *OH_10* (blue, dash-dotted), and *noHighT* (blue, dotted)

The modelled conversion of the emitted bromine into BrO and other forms is much slower when there are no radicals in the volcanic emission (*noHighT*). The bromine explosion takes tens of minutes to generate in-plume BrO/SO_2 ratios of order 10^{-4} in the *noHighT* run. . The bromine explosion initiates more quickly in most of the other runs with radical emissions, including the *br100_0* case with no volcanogenic Br radical emissions and only OH and NO radicals. These results highlight the importance of high-temperature-generated radicals to initiate the bromine explosion and generate modelled in-plume BrO/SO_2 ratios of the order observed. We also find low sensitivity to the initial speciation of bromine emissions in the model. We attribute this to halogen radicals (Br and Cl) being formed by reaction of volcanogenic OH with halides, these are sufficient to begin the autocatalytic chemistry even if no Br radicals are directly emitted at source. The output from the *OH_10* and *OH_25* runs appear to occupy an intermediate space between the quickly initiating runs and the slow *noHighT* case, suggesting that the radical emissions in these cases lie around the lower limit of radical emissions required for a quick initiation of the bromine explosion. Note however note that the model does not have any background bromine in any runs; in the absence of any volcanogenic radicals, such background bromine mixing into the plume could potentially contribute to initiating the autocatalytic processes. The exact abundance of radicals (e.g. OH, Br, Cl, NO) that may form by high-temperature reactions shortly after emission is not well known (Roberts et al., 2019).

Removing volcanic NO emissions from the model (run *NO_00*) results in moderately higher in-plume BrO in the early stages of plume evolution, as less bromine is held in the $BrNO_3$ reservoir. This difference dissipates with time, with the BrO/SO_2 ratios for the *NO_00* and *main* runs converging after a few 10s of minutes.

4.3 Chlorine species

The uptake to particles and subsequent reaction of HOBr with hydrogen halides (HBr, HCl) has the effect of transferring halogen from halides to reactive forms. When HBr and HCl are both present in the plume the product of this is almost exclusively Br_2 . However after a short time HBr is almost totally depleted in the plume and is consumed as fast as it is produced, whereas HCl remains abundant — the in-plume ratio of HCl to the inert tracer does not significantly change from the emission ratio in the study domain. The subsequent photolysis of BrCl produces reactive chlorine. This reactive chlorine forms the spectroscopically detectable species ClO and OClO within the plume — the reaction of Cl with ozone produces ClO, and the reaction of ClO with BrO produces OClO. Figure 13 shows the vertical columns of these species within the plume as ratios of the SO_2 column. ClO/SO_2 ratios are of similar magnitudes (a few 10^{-4}) to BrO/SO_2. $OClO/SO_2$ ratios are about two orders of magnitude lower, except for very close to the emission point where they are approach 1×10^{-5}.

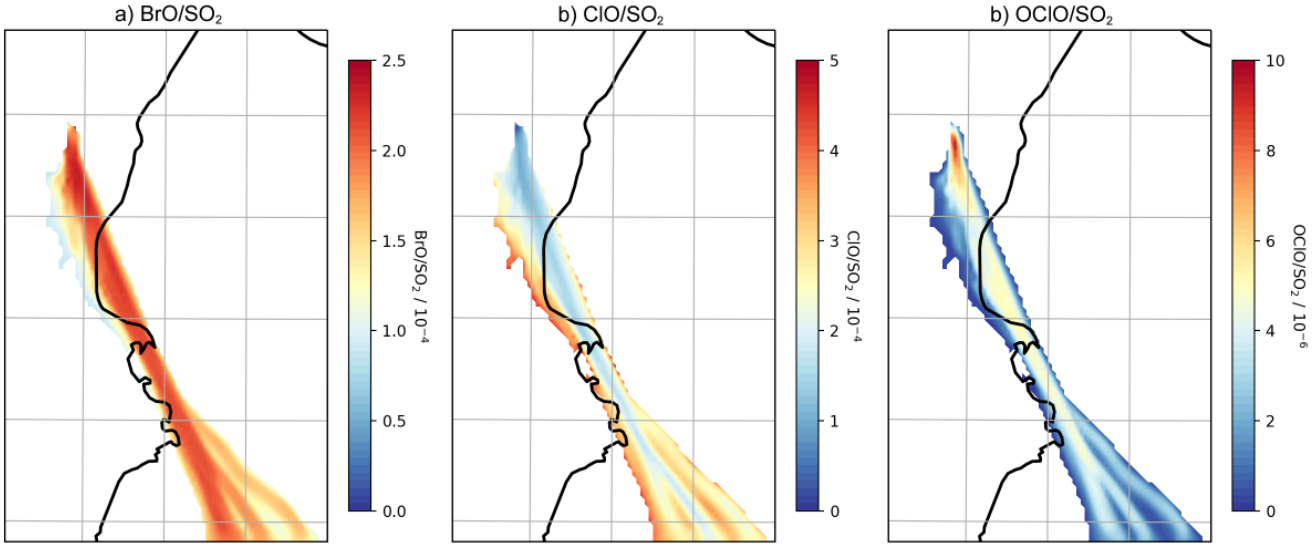

Figure 13. Model column ratios at 0800 UTC on 2012-08-01: a) BrO/SO_2, b) ClO/SO_2 c) $OClO/SO_2$. Only columns with a modelled SO_2 density greater than 2×10^{16} are plotted.

Spatially, lower ClO/SO_2 column ratios are found in the more concentrated parts of the plume (and higher ClO/SO_2 at the plume edges). Conversely, $OClO/SO_2$ shows the opposite spatial pattern, and is highest shortly after emission, because of the initial burst in OClO production from ClO and BrO in the concentrated early plume.

OClO and ClO are rarely observed above instrumental detection limits in volcanic plumes. Our model results are broadly consistent in magnitude with the few reported OClO observations in in Etna plume reaching 1×10^{-5} (Gliß et al., 2015) whilst General et al. (2014) report OClO/SO_2 up to 10^{-4} mol/mol. Some observational studies (Bobrowski et al., 2007; General et al., 2014) report greater BrO/SO_2 and OClO/SO_2 at the plume edges compared to the centre, which is not seen in our model. This might be due to the horizontal spatial resolution of WCV, or it might reflect a real difference in the chemistry of the plume. Note that box-modeling findings indicate that the magnitude of such 'edge effects' depends on volcanic conditions such as emitted the HBr/SO_2 (Roberts et al., 2018).

High levels of CH_4-oxidising chlorine radicals (Cl) in the plume reduce the instantaneous lifetime of CH_4 in the plume, which, in the early plume considered here, more than compensates for the decrease in CH_4 oxidation from the reduced levels of OH. However, at the edges of the plume, the lifetime-extending effect is greater, leading to the spatial pattern seen in Figure S4. Oxidation of CH_4 produces HCHO, and therefore the plume has elevated mixing ratios of this species (Figure S5).

4.4 Ozone depletion

During the day, ozone levels are lower in the plume than in the surrounding air (Figure 14). On the 30th, the in-plume ozone loss is only a few ppbv, whereas it reaches of the order of a few 10s of ppbv on the 31st and 1st. In terms of ozone columns, the maximum depletions modelled are of order of a few 10^{16} molec cm^{-2}.

Comparing output from the *main* and *novolc* model runs allows for a precise calculation of ΔO_3, the change in ozone due to the volcano. Following the approach used in Kelly et al. (2013) and Surl et al. (2015), we compute $\Delta O_3/SO_2$ to isolate the chemical signal from physical dispersion effects. Figure 15 shows the variation of this ratio with plume age at different times of day. Because this ozone destruction is slower on the 30th compared to the other two days, and because the plume is travelling faster due to the greater wind speed, the smaller ozone loss on 30th compared to the other days is even more apparent if $\Delta O_3/SO_2$ is plotted against distance (Figure 16). The absence of halogen chemistry means that, at night, $\Delta O_3/SO_2$ is close to zero. During the day the ratio is negative, and increases in magnitude with plume age. This indicates that chemical ozone destruction in the plume is a continuous, ongoing, process. Although the data depicted in Figure 15 are Eulerian snapshots rather than Lagrangian traces of the plume, these lines' gradients are an indication of the rate of the ozone loss process. For 2012-08-01 08:00, the gradient is about -7.5×10^{-6} molecules of O_3 per molecule SO_2 per second.

Secondly, by inspecting the rates of reaction for the *main* model run as shown in Figure S3, and computing the differences between the rates of ozone-destructive and ozone-forming reactions, we find that these halogen reactions result in an average net ozone loss rate of 3.1×10^7 molec cm^{-3} s^{-1} within this part of plume. Dividing this by the weighted average plume SO_2 mixing ratio yields an instantaneous loss rate of of 7.1×10^{-6} molecules of O_3 per molecule SO_2 per second, very close to the value determined by the prior method.

4.4.1 Attribution of ozone loss to halogen reactions

A detailed analysis of the model outputs allows us to attribute ozone loss to specific bromine reaction cycles. Ozone is destroyed by its reaction with Br to form BrO, but the net ozone loss depends on the subsequent fates of BrO and HOBr (the product of

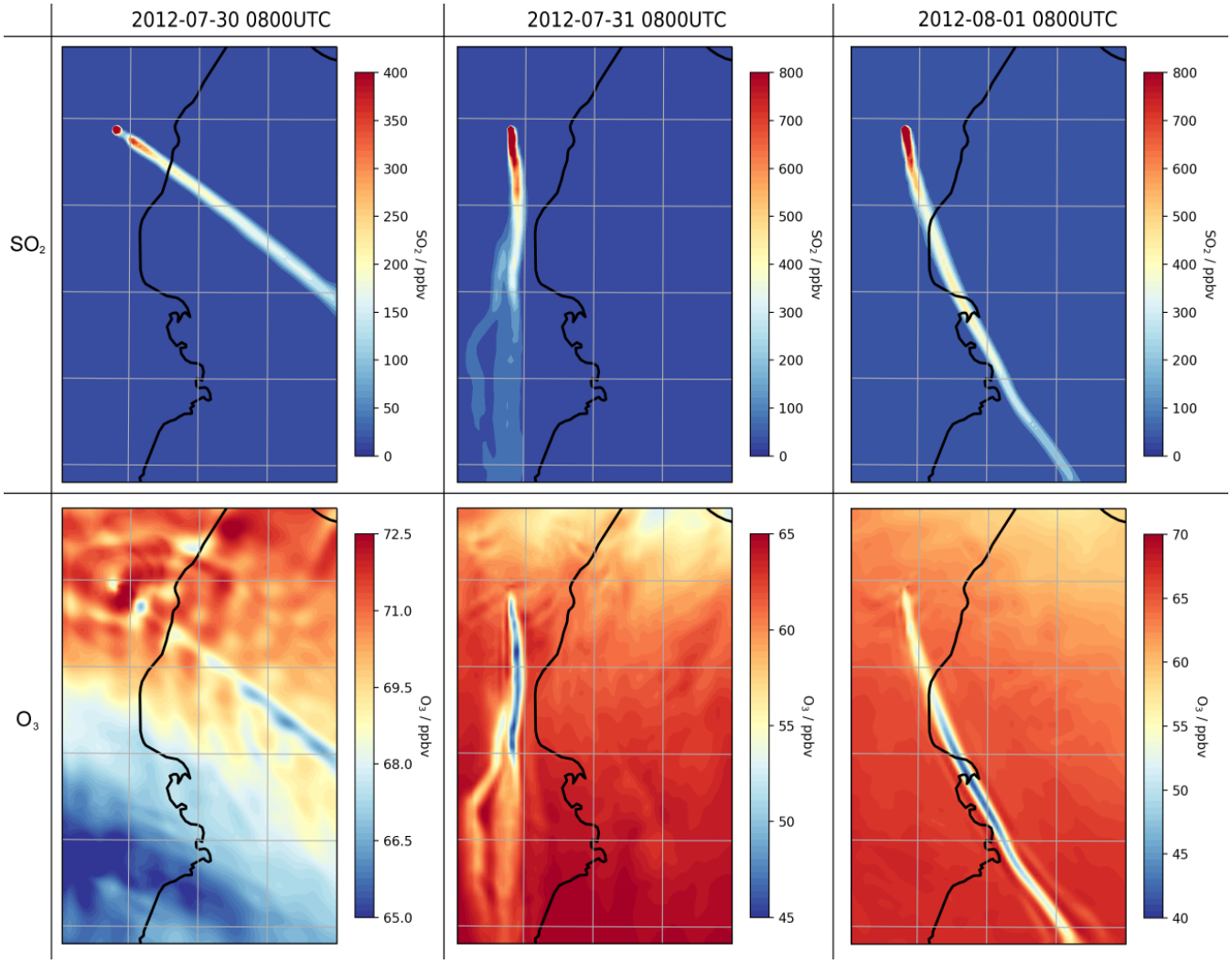

Figure 14. Modelled mixing ratios of SO_2 (first row) and O_3 (second row) at 3300mASL (volcano height) in the model at 0800 UTC on 2012-07-30 (first column), 2012-07-31 (second column), and 2012-08-01 (third column). Different colour scales are used for each subplot

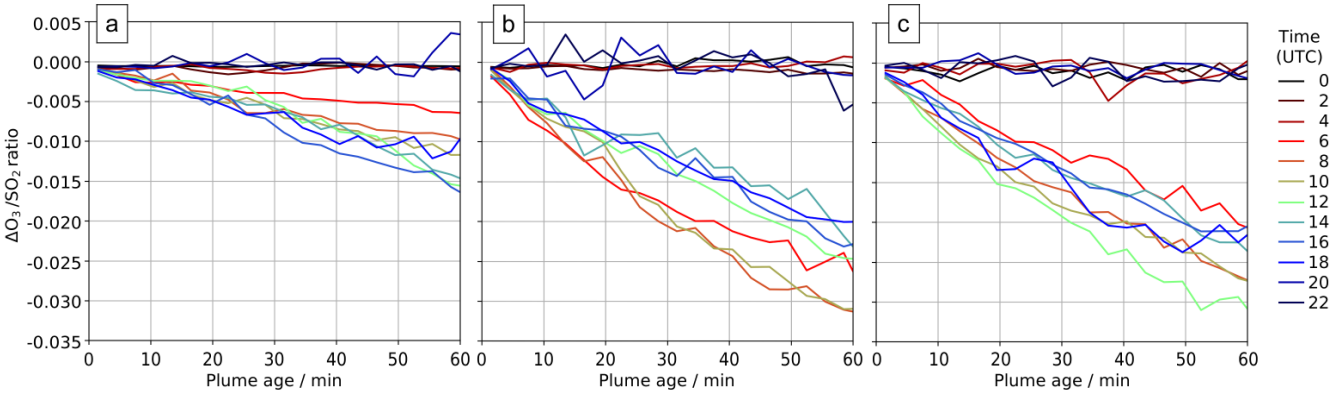

Figure 15. In-plume average $\Delta O_3/SO_2$ ratios for plume of different ages ranging from 0–60 minutes, at several times on a) 2012-07-30, b) 2012-07-31, and c) 2012-08-01. Only ratios where the corresponding SO_2 column exceeds 2.0×10^{16} molec cm^{-2} are shown.

Reaction	Fraction at plume age...			
	15min	30min	45min	90min
$BrO + BrO \longrightarrow 2\,Br$ or $Br_2 + O_2$	44%	40%	34%	28%
$BrO + ClO \longrightarrow Br + Cl$ or $BrCl + O_2$	21%	21%	22%	22%
$BrO + ClO \longrightarrow OClO + Br$	21%	21%	21%	25%
$BrO + NO \longrightarrow Br + NO_2$	1%	1%	1%	1%
$BrO + CH_3O_2 \longrightarrow Br + HCHO + HO_2$	1%	2%	3%	4%
$HOBr \xrightarrow{hv} Br + OH$	5%	8%	11%	13%
$HOBr + HBr \xrightarrow{het} Br_2 + H_2O$	2%	2%	2%	3%
$HOBr + HCl \xrightarrow{het} BrCl + H_2O$	6%	4%	6%	6%

Table 4. Modelled relative fractions of bromine reduction by the various non-O_3 forming reactions for plume of difference ages ($\pm$5 mins listed age) at 2012-08-01 08:00

BrO and HO_2). If BrO undergoes a reduction chemistry that reforms ozone there is no net impact, while if a reduction path does not reform ozone there is a net ozone loss. Table 4 tabulates the relative rates of the BrO and HOBr reduction reactions which yield Br, Br_2, or BrCl without reforming ozone in the plume and therefore can be "credited" with ozone destruction. We find that for this young plume, the most important of these bromine reduction reactions are the reactions of BrO with itself and of BrO with ClO, which together account for about three-quarters of the bromine recycling.

The relative importance of the BrO self-reaction decreases slightly as the plume dissipates and evolves, whilst the two reactions of BrO with ClO maintain the approximately same level of importance. The importance of HOBr photolysis increases over time but remains minor. Although the reactions of HOBr are responsible for only a minor fraction of the bromine reduction in this case, the heterogenous reactions of HOBr are important for transferring bromine from HBr and HOBr to the more potent ozone destructive forms, and for generating the reactive chlorine involved in the BrO + ClO reactions.

The overall rate of ozone destruction within the plume is dependent upon the quantity of bromine cycling. As shown in Figure 9, compared to the 30th, bromine is transferred faster out of HBr and $BrNO_3$ on the 31st and 1st as these are denser (more concentrated) plumes with higher surface area density. Additionally, because several of the reactions listed in Table 4 are between halogen species originating from the volcanic emissions, these are faster in denser plumes. As discussed in Section 4.1, the plume is less dense on the 30th due to the higher wind causing volcanic emissions to be injected in larger volumes of air and greater dilution of volcanic emissions. These factors result in a slower ozone destruction for 30th, as shown in Figure 15a. Because this ozone destruction is slower, but the plume travels faster, this difference is magnified if $\Delta O_3/SO_2$ is plotted against distance (as is done in Figure 16).

4.4.2 Comparison of model and aircraft data on ozone loss

Here we compare the aircraft observations to model outputs. Because the model plume does not precisely trace the same path as the observed plume, using the exact coordinates of each in-plume observation to identify the plume in the model domain would certainly often result in missing the modelled plume. Instead, for each of the plume encounters discussed in Section 3, we identify the equivalent of the observations in the model by the following method. Model data are considered "equivalent" for a plume encounter if they satisfy the following criteria:

- Time is closest to the median time of the observed encounter.
- Grid box is wholly or in part within the altitude range of the observed plume encounter.
- Grid box centre is within the range of distances from Etna for the observed plume encounter.
- SO_2 mixing ratio is in excess of 10 ppbv.

This effectively delimits a 3D space within the model. This 3D space is more likely to include the most concentrated part of the plume than the 1D transect made by the aircraft, and as such, the model data tends to include grid boxes with SO_2 greater than the maximum values from the observed plume encounter. For this reason our observation-model comparisons are based on O_3 vs. SO_2 trends rather than absolute values.

The model output is hourly, and the looping flight path (Figure 2) means that many of the plume encounters were made minutes apart at nearly the same points in space. As a result, several of these model-equivalent sets share many model data points and are nearly identical. Model equivalents of Figures 4 and 5 are shown, respectively, in Figures S8 and S9. The coefficients from simple linear regression of these data are tabulated in Table 5.

The gradients of $\Delta O_3/SO_2$ versus plume age from applying a linear regression to the model and observation data are very similar. Weighting by the quantity and R^2 of the fit of the observational data, the root mean square difference of the two gradients is 0.005, with a weighted mean bias of less than 0.001. Figure 16 plots modelled $\Delta O_3/SO_2$ and these plume encounter gradients against distance from the volcano. The range of distances of the plume encounters is insufficient to determine any trend from the observations beyond those made in Section 3, however there is a reasonable match between observed and

#	Observation								Model		
	Day	time (UTC)	dur. /s	alt. / mASL	dist. / km	grad.	int. / ppbv	R^2	grad.	int. / ppbv	R^2
1	31	07:41:01–07:49:11	500	3596–3748	10.2–14.7	-0.020	47.1	0.20	-0.019	68.2	0.77
2	31	07:51:00–07:54:40	230	3699–3779	8.5–13.4	-0.011	48.6	0.53	-0.017	69.2	0.80
3	31	07:54:50–07:58:00	200	3700–3782	7.2–12.0	-0.006	49.2	0.06	-0.016	69.9	0.82
4	31	07:58:11–08:06:10	490	3555–3719	9.6–14.4	-0.025	51.9	0.44	-0.019	68.4	0.79
5	31	08:06:21–08:15:10	540	3466–3591	10.5–15.2	-0.016	50.0	0.50	-0.019	67.0	0.79
6	31	08:16:50–08:20:01	200	3484–3516	10.6–15.6	-0.022	50.4	0.51	-0.021	66.8	0.86
7	31	08:20:10–08:22:31	150	3466–3643	13.0–17.4	-0.007	46.9	0.19	-0.021	65.7	0.84
8	31	08:22:40–08:25:11	160	3567–3658	14.2–19.0	-0.023	48.1	0.71	-0.026	66.4	0.82
9	31	08:27:11–08:32:20	320	3597–3724	16.4–21.2	-0.025	48.5	0.80	-0.027	68.2	0.78
10	31	08:32:31–08:34:20	120	3623–3657	12.9–17.4	+0.009	42.1	0.23	-0.024	66.0	0.86
11	31	08:36:11–08:41:11	310	3604–3698	9.9–14.7	-0.003	43.4	0.16	-0.021	68.2	0.77
12	1	06:48:44–06:51:43	190	3090–3387	12.5–16.8	+0.006	49.2	0.11	-0.018	65.8	0.67
13	1	06:51:54–06:56:04	260	3430–3646	11.8–16.8	-0.019	51.0	0.54	-0.017	68.9	0.88
14	1	06:56:13–07:04:04	480	3486–3548	11.7–16.6	-0.017	50.4	0.65	-0.017	68.8	0.86
15	1	07:04:13–07:08:24	260	3506–3561	12.5–17.4	-0.015	50.9	0.81	-0.018	68.7	0.89
16	1	07:08:33–07:11:13	170	3510–3543	11.7–16.5	-0.020	51.7	0.67	-0.017	68.8	0.86
17	1	07:11:24–07:13:53	160	3490–3560	11.2–15.9	-0.014	48.8	0.91	-0.016	69.1	0.81
18	1	07:14:04–07:21:23	450	3420–3581	10.1–15.1	-0.019	51.2	0.75	-0.017	69.3	0.76
19	1	07:21:34–07:23:34	130	3249–3498	7.6–10.0	-0.046	53.4	0.97	-0.011	68.1	0.67

Table 5. Data relating to the major plume encounters, and the equivalent model data, depicted in Figures 4 and 5 (observations) and Figures S8 and S9 (model). dur = duration of plume encounter, alt = range of altitudes of plume encounter, dist = distance from Etna, grad = gradient of line-of-best fit of O_3 vs. SO_2 slope, int = y-intercept of this line

modelled $\Delta O_3/SO_2$ values for distances of around 15 km from the volcano. This gives confidence that the model has skill with regards to the ozone chemistry of the plume.

The y-intercept of the lines of best fit in the model are consistently 15–20 ppbv lower than those of the observations, reflecting a somewhat higher background ozone. The cause of this is most likely bias in the initial and boundary conditions used in the model. We do not expect this offset to have a significant impact on the main results of this study, which are based on changes in ozone, (ΔO_3), rather than its absolute magnitude.

4.4.3 Relationship of ozone losses to the magnitude of halogen emissions

As tabulated in Table 2, we ran the model with different volcanic fluxes in order to assess how volcanic impacts on ozone could vary for different passive degassing emission compositions. In Table 6 we report, for the *main*, *mag*, *hal*, and *oth* runs the average ΔO_3 values (compared to the *novolc* run) in ppbv for modelled plume aged 60 ± 5 minutes at 2012-08-01 08:00 as

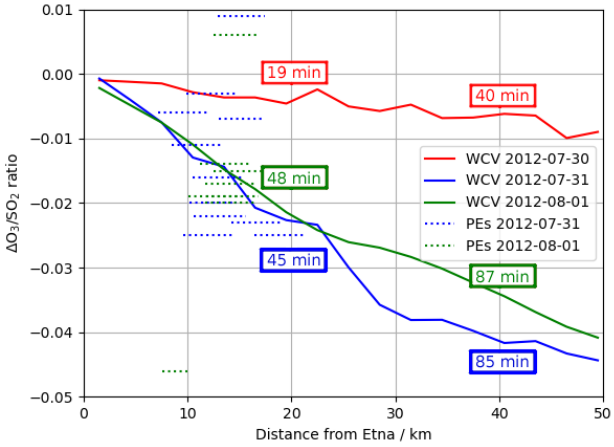

Figure 16. Modelled $\Delta O_3/SO_2$ ratios at 0800 UTC on 2012-07-30, 2012-07-31, and 2012-07-31 (solid lines), and observed O_3 vs. SO_2 gradient from each of the major plume encounters (dashed lines), plotted against distance from the volcano. Observations are plotted as horizontal lines spanning the range of distances from the volcano at for the plume encounter. Annotations give the average age of the modelled plumes at 20 and 40 km distances.

a metric for the volcanic impact on ozone. Collectively, these runs explore a two-dimensional parameter space of variations in halogen and other emissions. In all these runs the chlorine emission is scaled to the bromine emission (Cl/Br = 300 by mass), the bromine is emitted in the same 3:1 fixed proportions of HBr and Br, and all other species (H_2O, Hg, OH, NO, at-source aerosol) are scaled to the SO_2 emission. In the absence of both SO_2 and bromine emissions the ozone loss relative to the *novolc*

		Bromine emissions g s^{-1}			
		0	10	30	45
SO_2 emissions kg s^{-1}	0	0			
	13		-1.1	-5.5	
	40	0.6	-1.3	-7.2	-13.4
	60			-7.3	-13.3

Table 6. ΔO_3 values (compared to *novolc* run) in ppbv for plume aged 60 ± 5 minutes at 2012-08-01 08:00 for various model runs with varying emissions. For all runs the Cl/Br, Br/HBr, OH/SO_2, NO/SO_2, H_2O/SO_2, Hg/SO_2, and aerosol/SO_2 emission ratios remain the same as in *main*. The 40 kg s^{-1} row and 30 g s^{-1} column indicate the emission fluxes used in *main*.

run is, by definition, zero. For the volcanic case without halogens (i.e. the *hal00* case), there is a slight ozone production in the plume, as shown in Table 6; model cells for 1-hour old plumes have, on average, about half a ppbv more O_3 than the equivalent cells in the totally plume free case. We ascribe this phenomenon to the impact of the volcanic NO emissions which results in tropospheric ozone-production during NO_x cycling. Table 6 confirms that it is the halogen emission that causes the ozone loss.

Increasing the modelled flux of all species other than the halogens above that of the *main* case does not significantly change the depletion amounts. However, decreasing this flux by two-thirds reduces ozone depletion by around 20%. As was the case for the 30th in the *main* model run, the surface area density is insufficient to quickly move bromine from HBr to the ozone-destructive cycle – though in this case this is due to weaker aerosol emissions rather than faster wind speeds.

The four data points for different bromine fluxes at 40 kg SO_2 s^{-1} can be fitted to a second order polynomial, $(\Delta O_3)_{60min} = -3.5 \times 10^{-3}x^2 - 0.15x + 0.6$ ppbv, where x is the volcanic bromine flux in g s^{-1}. We interpret this combination of a second- and first-order terms to be the product of the complexities of the chemistry. The reactions that recycle BrO through reaction with other halogen oxide species would be expected to have rates approximately proportional to the square of the amount of halogens in the plume, while the rates of those that recycle HOBr, including those that generate reactive halogens from hydrogen halides, would vary approximately linearly with this quantity.

We caution against scaling these results to the plumes of large eruptions. Such plumes could have near-total depletion of ozone and/or HO_x and produce non-linear effects beyond the scope of this study. The halogen chemistry of large eruptions is being investigated using the WCV model and will be the focus of a future study.

To conclude this study on passively degassing plumes, we analyse the WCV model outputs to highlight how volcanic halogens also impact nitrogen and mercury species

4.5 NO_x, NO_y, and nitrate aerosol

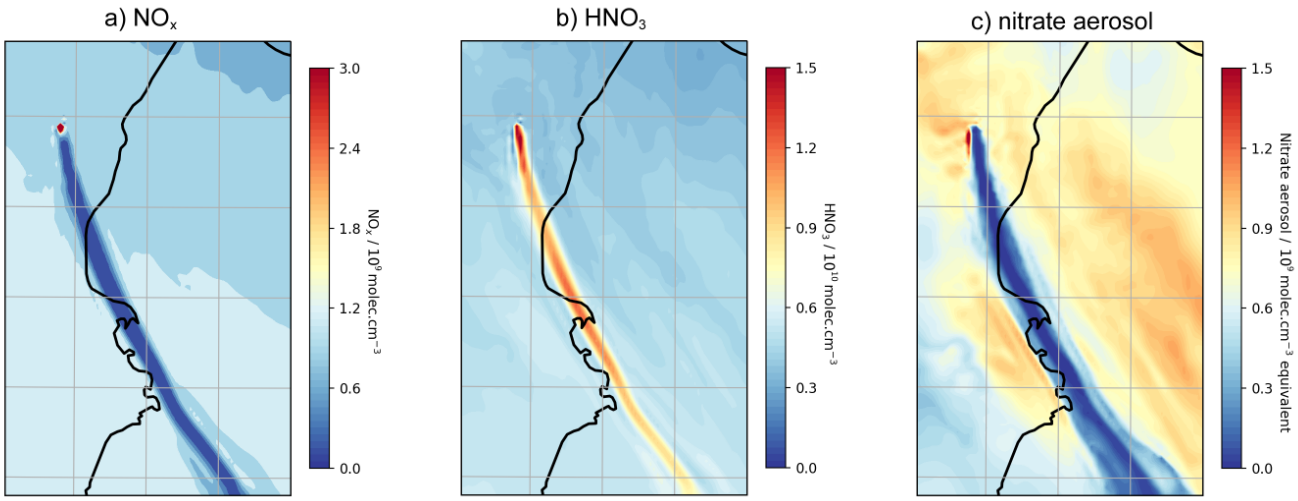

Figure 17. a) model mixing ratio of NO_x, b) model mixing ratio of HNO_3, c) equivalent mixing ratio of aerosol-phase nitrate at 3300mASL in the model at 0800 UTC on 2012-08-01.

Although the volcano degassing is a source of NO in the model, the core of the plume is nearly totally depleted in NO_x, with concentrations of less than 10^8 molec cm^{-3} compared to background concentrations of around 10^9 molec cm^{-3} (Figure 17a).

The reason for plume NO_x being below background levels is the reaction sequence BrO + NO_2 $\longrightarrow$ $BrNO_3$ followed by the heterogeneous reaction of $BrNO_3$ with hydrogen halide that has the net effect of converting NO_2 into HNO_3, a phenomenon discussed by Roberts et al. (2014). As a consequence, as shown in Figure 17b, the plume is elevated in HNO_3 compared to the background — the average in-plume HNO_3 concentration is around $13–16 \times 10^9$ molec cm^{-3} compared to $7–8 \times 10^9$ molec cm^{-3} in the background. Elevated HNO_3 has been observed in a number of volcanic plumes (Mather et al., 2004a, b; Martin et al., 2012; Voigt et al., 2014).

As well as the conversion of the volcanogenic and background NO_x, displacement of nitrate from background aerosol can also contribute to the in-plume HNO_3. The acidic plume, rich in sulfuric and hydrochloric acid, displaces nitrate from background aerosol into the gas phase as HNO_3. As shown in Figure 17c, the aerosol-phase nitrate content within the plume is much lower than the background in the model. The contributions of background NO_x (via $BrNO_3$) and background nitrate (via acid displacement) to the plume HNO_3 enhancement are of similar magnitude. Because of the conversion of background species, the volcano is not required to be a source of NO_x for in-plume HNO_3 elevation to occur. In the *NO_00* model run, the plume is still elevated in HNO_3 due to conversion of background N (Figure S7), the magnitude of this is about half that of the *main* case.

As discussed by Martin et al. (2012) it is unclear from reaction kinetics if volcanoes are sources of reactive nitrogen. The levels of background NO_x and nitrate aerosol in the free-tropospheric environment modelled in this study (July–August 2012) would be too low to yield, by themselves, HNO_3 concentrations of the order measured by (Mather et al., 2004a) at Mount Etna summit in May 2002, nor those measured in the plume of Etna in a September 2011 aircraft campaign (Voigt et al., 2014). However background NO_x and nitrate may be significant contributors to volcanic HNO_3 in more nitrogen-polluted environments. Voigt et al. (2014) states that typical conversion times of atmospheric NO_x to HNO_3 is days in summer mid-latitudes, and so cannot explain formation of HNO_3 in volcanic plumes. Our modelling results show in-plume gas-phase HNO_3 being generated quickly by the mechanisms of acid displacement of background nitrate aerosol and volcanic plume halogen chemistry that converts background NO_x as well as volcanic NO_x (if present) into HNO_3 via $BrNO_3$. These results suggest that analyses of HNO_3 measurements within plumes used to assess volcanogenic NO_x or NO_y need to account for background reactive nitrogen in both the gas and particulate phases.

Due to the formation of the $BrNO_3$ reservoir, a volcanic NO_x emission (or, potentially, background NO_x of similar magnitude to the plume bromine) could impact the bromine chemistry and speciation and limit the amount of reactive bromine available to form BrO. The quantity of $BrNO_3$ that accumulates depends upon the abundance of NO_x available to react with BrO and the rate at which $BrNO_3$ decays via heterogeneous chemistry. Of the three days modelled, only on the 30th, where the in-plume heterogeneous rates are low (due to a higher windspeed causing greater along-plume dilution), is a substantial fraction of plume bromine held in the $BrNO_3$ reservoir for several minutes.

4.6 Halogen impacts on mercury

The volcano is modelled to emit, per mol of SO_2, 7.8×10^{-6} mol of Hg in an unoxidised state. A simplified Hg chemistry scheme has been implemented in WCV to evaluate the extent to which this Hg can become oxidised by interaction with the

volcanic halogen chemistry. Importantly, our mechanism includes the recently identified photo-reduction pathways of Hg(I)-halides (Saiz-Lopez et al., 2019). For the purposes of this study focused on halogens only, other possible mercury oxidation pathways are ignored. Due to the relatively low quantity of Hg in the plume, the effect of Hg on the halogen chemistry system itself is negligible.

675 Figure 18 shows the instantaneous average in-plume rates of reactions in the mercury cycle for plume aged 40-50 minutes at 2012-08-01 1200 UTC. Although there is a moderately fast oxidation of Hg to HgBr and HgCl, this is mostly offset by reduction. In agreement with global modeling of Saiz-Lopez et al. (2019), photolysis is the dominant Hg(I) reduction process. Overall, there is a small net oxidation of Hg occurring in the plume, but it is slow — for daytime plumes the average in-plume lifetime of Hg(0) is of the order of a few hours and this oxidation is mostly offset by photo-reduction. Despite the slow rate

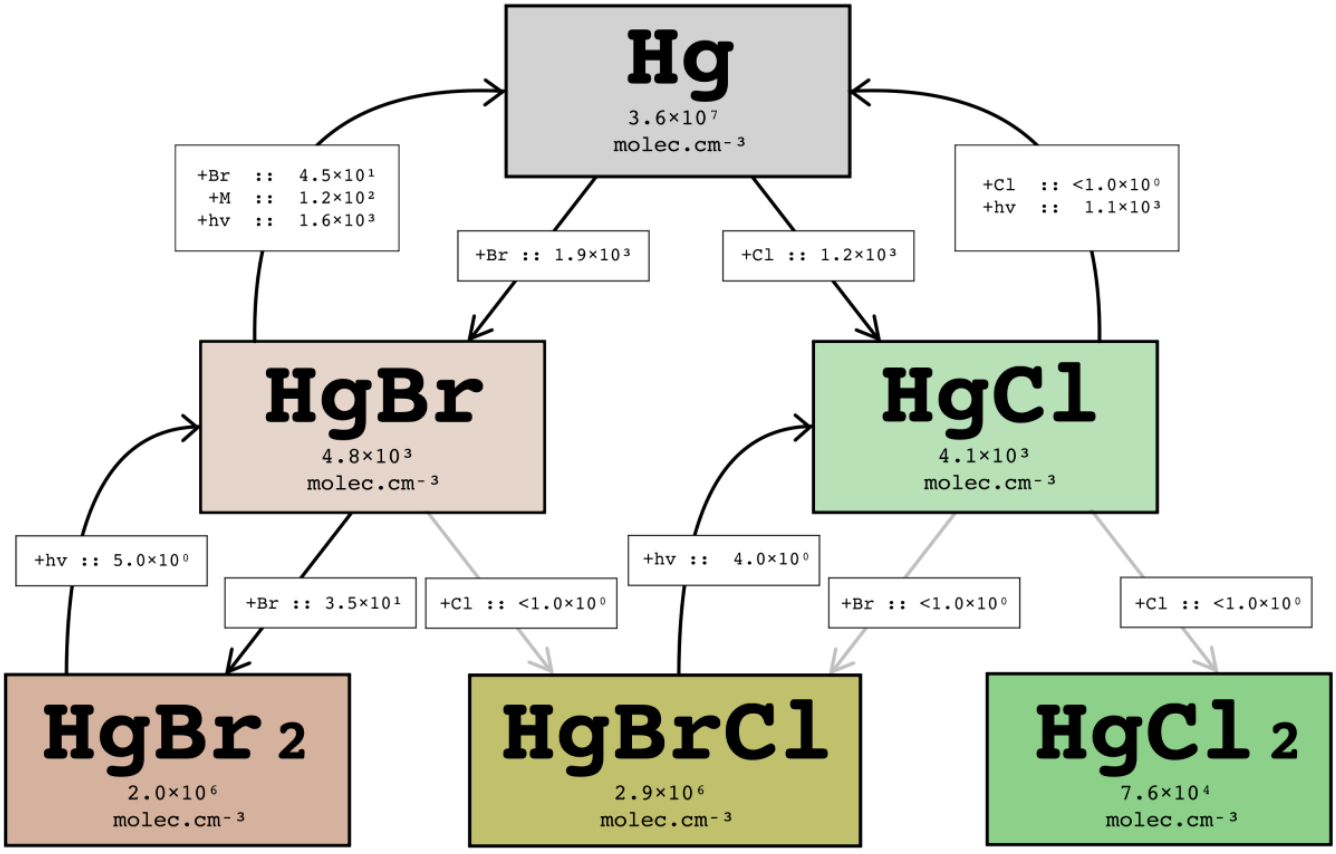

Figure 18. Instantaneous average in-plume concentrations and reaction rates (in molec cm^{-3} s^{-1}) for the Hg cycle for plume aged 40-50 minutes at 2012-08-01 1200 UTC. Rates less than 1 molec cm^{-3} s^{-1} are written as $<1.0 \times 10^0$.

680 of oxidation in the plumes aged 10s of minutes, we find that in the early plume, modelled levels of mercury oxidation can be several % (Figure S6) from the first few minutes of evolution during both night and day. We attribute this oxidised mercury to

oxidation occurring in the very early plume (first few seconds) where volcanogenic radicals are in high concentrations. This near instantaneous oxidation accounts for the vast majority of oxidised mercury in the modelled plume further downwind. Supporting this interpretation, we find negligible Hg oxidation in the first hour of plume evolution in output the *noHighT* run. Therefore variations in the Hg oxidation with plume age and time of day are due mostly the conditions at the point of emission, rather than any processes occurring within the downwind plume.

We conclude that, for our case study of a Mount Etna passive degassing plume that focused on mercury-halogen interactions only, the net in-plume oxidation rate of mercury by halogen chemistry is near-negligible in the dispersed plume but could be significant very close to the source. Our findings contrast with the model study of von Glasow (2010) that predicted substantial oxidation of mercury to Hg(II) occurring in the dispersed volcanic plume of Mount Etna. However, that study did not include the very fast HgCl and HgBr photo-reduction pathways that critically impact the overall Hg oxidation, although it did include a SO_2-mediated reduction of Hg(II) hypothesised by (Seigneur et al., 2006). We note that this slow net oxidation rate in the modelled evolved plume occurs despite the absence of this reduction pathway in the mechanism.

We invite caution regarding the interpretation of these results due to the very simple mercury chemical scheme used, and the apparent importance of the first few seconds of plume evolution which would be, spatially, poorly represented even at 1 km grid resolution.

Further investigation of mercury chemistry in volcanic plumes is needed, across a range of volcanic and meteorological conditions. This requires modeling at higher resolution to capture very near source processes both in the young cooled plume as well as investigations of hot plume chemistry just after emission, and the mercury chemistry in much larger eruption plumes that may differ from passive degassing case. The mercury oxidation-reduction scheme should also be extended to investigate possible roles of other gases (e.g. NO_x). More comprehensive observation studies of speciated mercury at Mount Etna and other volcanoes are also needed.

5 Conclusions

Volcanoes emit halogens that are converted into active chemical radicals in plumes and whose chemistry, notably bromine, causes ozone destruction. However, the plume processes driving this halogen conversion, the so-called halogen activation, and the ensuing ozone depletion within the volcanic plumes are not yet well constrained by the limited observational datasets and numerical model studies. It remains difficult to assess accurately the large-scale impact of volcanic halogens without a quantitative understanding of halogen plume chemistry. This study presents a new dataset of airborne measurements made during the summer 2012 in the degassing plume from the Mount Etna volcano, up to a few 10s of km from the source. This chemically reactive plume is simulated using a new numerical 3D model "WRF-Chem Volcano" (WCV), a version of WRF-Chem we have modified to incorporate volcanic emissions (including HBr and HCl) and multi-phase halogen chemistry.

Measurements of SO_2 and ozone levels in the plume are found to be strongly anticorrelated. Ozone losses reach of up to about 10 ppbv. Accounting for the distance from the source at which these measurements were taken (7–21 km downwind from the summit), and using modelled wind speeds, the ozone destruction rate is estimated at approximately 1.3×10^{-5} mol

O_3 per mol SO_2 per second. This value is similar to observation-derived estimates reported very close to the Mount Etna vents (<500 m downwind) (Surl et al., 2015), indicating continual ozone loss in the plume up to 10's km downwind.

The aircraft observations are analysed with the WCV model forced by emission fluxes of volcanic gases, including SO_2, mercury, and halogens (HBr, HCl), each set to values within typical ranges observed for Etna in a passive degassing state. The model initialization also includes a representation of high-temperature radicals (Br, OH, NO) and a volcanic sulfate particle emission. The WCV mechanism includes photolytic, gas-phase and multi-phase reactions of bromine and chlorine, as well as gas-phase oxidation of SO_2. WCV was run using two-way nested grids, enabling 1 km resolution for the simulation of plume processes close to the volcano — the focus of this study.

The model simulates the in-plume conversion of emitted HBr into halogen radicals such as BrO, and ozone destruction in the volcanic plume. Modelled in-plume BrO/SO_2 columns are similar to those observed at Mount Etna and other volcanoes, both in terms of magnitude (molar ratio of around 10^{-4}) and their spatial variation (rise and plateau with distance downwind). For modelled plume corresponding to the observations the resulting O_3 versus SO_2 gradients are very similar to those in the observational data. We compute ΔO_3, the modelled ozone change due to the plume, by comparing output from model runs with and without volcanic emissions. The variation of $\Delta O_3/SO_2$ ratios with plume age yields the rate of ozone loss as a ratio of SO_2. At the time of the plume measurements on 2012-08-01, this quantity is approximately 7.5×10^{-6} molec molec^{-1} s^{-1}, with a very similar value from an analysis of the instantaneous rates of reactions. In summary, the WCV model shows apparent skill in reproducing plume halogen chemistry and impacts on tropospheric ozone.

Inspecting the bromine chemical system, we found that HBr, the dominant form of bromine at emission, is converted to other forms within the first few minutes of plume evolution. These forms undergo a continuous cycling in the plume, with with BrO and HOBr being the dominant daytime forms. We found that a lower plume density, caused by a greater wind speed, slowed the evolution of the bromine chemical system with more bromine residing in HBr, HOBr, and $BrNO_3$. The balance between BrO and HOBr varies moderately with time of day due to diurnal variations in HO_2, yielding slightly lower BrO/SO_2 around solar noon. Inspection of the rates of reaction find that although the overall proportions of bromine in different forms stabilises after a few 10s of minutes of plume evolution, bromine is constantly cycling between forms, and this process includes the ozone destructive Br + O_3 $\longrightarrow$ BrO reaction. Overall the ozone loss depends on several different reactions that reduce oxidised bromine without recreating ozone. We find that, for young plumes (<1 hour old), the most important reactions are those of BrO with halogen monoxides (BrO or ClO).

The conversion of volcanic HBr into reactive bromine forms occurs by the heterogeneous reaction of HOBr. Once plume HBr is depleted, this reaction acts to convert HCl into reactive chlorine, leading to the release of methane-oxidising chlorine radicals. As a result the lifetime of methane is reduced in the plume core, however at the plume edge methane lifetime increases due to lower OH. The CH_4 oxidation initates organic chemistry processing that results in formaldehyde being elevated in the plume compared to the background. Cl radicals also generate ClO and OClO — species that have also been detected in the plumes of some volcanoes including Mount Etna. Modelled near-source OClO/SO_2 ratios are of approximately similar magnitude (10^{-5} mol/mol) to those measured by Gliß et al. (2015).

The model plume chemistry is investigated over a range of emission scenarios. If the radical species expected to be produced in the high temperature volatile-air mix are excluded, the evolution of the halogen chemistry is greatly slowed and delayed. This result highlights the importance of understanding these very early processes in order to have an accurate picture of the overall chemistry. A sensitivity study of the model response to variations in the emissions of both halogens and sulfur finds that ozone loss depends on the bromine emission flux with both linear and quadratic components, reflecting the complexities of the plume chemistry.

Finally, the model outputs are inspected to identify halogen impacts on HO_x, sulfur, NO_x and mercury chemistry.

Despite the volcano being an initial source of high-temperature OH radicals, for the early (<1 hr age) plume considered in this study the in-plume instantaneous lifetime of SO_2 in the model is substantially increased (from about 2 days to about 2 weeks) due to depletion of OH. These modelling results therefore strengthen the case for using SO_2 as a plume tracer on these scales. The substantial depletion of OH is attributed to both SO_2 and halogen chemistry which further reduces OH concentrations within the plume. Halogen chemistry also causes depletion of HO_2.

The SO_2 oxidation that does occur nevertheless produces sulfate aerosol mass and surface area within the plume. Secondary aerosol is formed more quickly in a simulation that excludes volcanic halogens. This result demonstrates that volcanic halogen chemistry can critically influence sulfur oxidation processes, and emphasizes the need to include halogens in studies of volcanic sulfate aerosol impacts.

Despite the volcano being modelled as an initial source of high-T NO, modelled in-plume NO_x levels are lower than the surrounding air due to plume chemistry destroying these species. In-plume HNO_3 was found to be elevated for two reasons: bromine chemistry converts NO_x to HNO_3, and background aerosol-phase nitrate is displaced into the gas phase by the acidic plume.

The model includes a very simple mercury scheme which includes photolysis reduction of mercury halides. In this passively degassing case, WCV predicts some early-stage oxidation of mercury by the initial high-temperature region Br radicals, but — in contrast to previous model studies for Mount Etna passive degassing — also predicts a very slow net oxidation by halogens in the downwind plume. Further model-observation studies of volcanic mercury with more complete schemes are warranted, as well as lab experiments assessing the rates of atmospheric mercury reactions.

The rates of the various halogen reactions critical to the main results of this manuscript are reasonably well-known, with the significant exception of the heterogeneous processing of HOBr. The recommended effective uptake coefficient is based on experiments on surfaces that do not necessarily well-represent volcanic particles (Ammann et al., 2013). Additionally the surface area available for this reaction is strongly dependant on the quantity and character of volcanic particulate emissions. Such settings used in for the modelling of this work are very loosely constrained by observations from other time periods (Roberts et al., 2018) and the Summer 2012 emissions of Etna may vary substantially from these. Together with the simplistic assumption of spherical particles, there is overall a large uncertainty regarding this processing. An additional source of uncertainty is the extent to which WRF-Chem over-disperses the plume in the vertical dimension, a known problem with Eularian models (Lachatre et al., 2020). We note that the emission magnitude in the model was calibrated so as to approximately replicate the aircraft-observed mixing ratios of SO_2.

Overall, however, the WCV model appears to show reasonable skill in replicating observed in-plume phenomena of ozone loss specific to this case study and established downwind trends in BrO/SO_2 for minutes-old passive degassing plumes more generally. Deriving confidence from this, we believe that our model results are, at least, a reasonable representation of the halogen chemistry occurring within a passive degassing volcanic plume.

This skill gives credence to the assessments of the chemical processes occurring within the plume. WCV operated using nested-grids enables to reach 1 km resolution, however, we suggest caution in using results from the model for processes occurring at sub-km scale within the very early plume. This study investigated the chemical processes occurring in the passively degassing plume of Mount Etna. We caution against extrapolating these results to stronger (more dense) eruption plumes, as such plumes may experience phenomena out of scope of this study, such as near-total ozone depletion that perturbs the halogen chemistry. WCV is being applied in a follow-up study to investigate the plume chemical processes in such dense plumes from volcanic eruptions to the troposphere, as a contrast to this passive degassing case. In future, WCV can also be applied to assess the tropospheric impacts of volcanic halogen chemistry in plumes as they disperse and may remain chemically active for up to regional scales.

Code availability. Availability of model code

The code of WCV is available on GitHub (Surl, 2020). This repository is being actively maintained. The version of the code used to generate the results of this study are included in this repository as a static branch (`etna2012`).

The modifications to the PrepChem utility have been submitted to the maintainers of this software for consideration, and are available from the authors on request.

Data availability. Data availability

WRF-Chem generates NetCDF files as output. The output relating to the innermost domain (*d04* on Figure 3) are uploaded to a Zenodo online repository (Surl, 2021). This repository also contains the input settings files used for the runs.

Author contributions.

L.S. analysed the observational data, made the model code modifications, ran the model, and analysed and visualised the model output. All authors wrote the manuscript, provided critical feedback, and helped shape the research and analysis. T.R. supervised the project.

Competing interests.

The authors declare they have no competing interests.

Acknowledgements. This manuscript is a result of a project that has received funding from the European Union's Horizon 2020 research and innovation programme under grant agreement No 800062, as well as ANR Projet de Recherche Collaborative VOLC-HAL-CLIM (Volcanic Halogens: from Deep Earth to Atmospheric Impacts), ANR-18-CE01-0018.

Computer modeling benefited from access to IDRIS HPC resources (GENCI allocation A007017141) and the IPSL mesoscale computing center (CICLAD: Calcul Intensif pour le CLimat, l'Atmosphère et la Dynamique).

Aircraft measurements were carried out within the Global Mercury Observation System project (GMOS; www.gmos.eu) and we acknowledge the contribution of the GMOS teams of CNR IIA, Italy and Helmholtz-Zentrum Geesthacht, Germany. GMOS was financially supported by the European Union within the seventh framework programme (FP-7, Project ENV.2010.4.1.3-2).

The authors would like to thank Louis Marelle and Jennie Thomas for their assistance with the model development. The model presented in this manuscript is a development on work undertaken as part of Luke Surl's PhD which was funded by the UK's Natural Environment Research Council, and supervised by Deanna Donohoue and Roland von Glasow.

The authors would like to thank two anonymous referees for suggesting various improvements to this manuscript.

References

Aiuppa, A., Bellomo, S., D'Alessandro, W., Federico, C., Ferm, M., and Valenza, M.: Volcanic plume monitoring at Mount Etna by diffusive (passive) sampling, Journal of Geophysical Research: Atmospheres, 109, https://doi.org/10.1029/2003JD004481, 2004.

Aiuppa, A., Federico, C., Franco, A., Giudice, G., Gurrieri, S., Inguaggiato, S., Liuzzo, M., McGonigle, A. J. S., and Valenza, M.: Emission of bromine and iodine from Mount Etna volcano, Geochemistry Geophysics Geosystems, 6, https://doi.org/10.1029/2005gc000965, 2005.

Aiuppa, A., Franco, A., von Glasow, R., Allen, A. G., D'Alessandro, W., Mather, T. A., Pyle, D. M., and Valenza, M.: The tropospheric processing of acidic gases and hydrogen sulphide in volcanic gas plumes as inferred from field and model investigations, Atmospheric Chemistry and Physics, 7, 1441–1450, https://doi.org/10.5194/acp-7-1441-2007, 2007.

Aiuppa, A., Giudice, G., Gurrieri, S., Liuzzo, M., Burton, M., Caltabiano, T., McGonigle, A. J. S., Salerno, G., Shinohara, H., and Valenza, M.: Total volatile flux from Mount Etna, Geophysical Research Letters, 35, https://doi.org/10.1029/2008GL035871, 2008.

Ammann, M., Cox, R. A., Crowley, J. N., Jenkin, M. E., Mellouki, A., Rossi, M. J., Troe, J., and Wallington, T. J.: Evaluated kinetic and photochemical data for atmospheric chemistry: Volume VI - heterogeneous reactions with liquid substrates, Atmospheric Chemistry and Physics, 13, 8045–8228, https://doi.org/10.5194/acp-13-8045-2013, 2013.

Badia, A., Reeves, C. E., Baker, A. R., Saiz-Lopez, A., Volkamer, R., Koenig, T. K., Apel, E. C., Hornbrook, R. S., Carpenter, L. J., Andrews, S. J., Sherwen, T., and von Glasow, R.: Importance of reactive halogens in the tropical marine atmosphere: a regional modelling study using WRF-Chem, Atmospheric Chemistry and Physics, 19, 3161–3189, https://doi.org/10.5194/acp-19-3161-2019, 2019.

Bagnato, E., Aiuppa, A., Parello, F., Calabrese, S., D'Alessandro, W., T.A., M., McGonigle, A., Pyle, D., and Wängberg, I.: Degassing of gaseous (elemental and reactive) and particulate mercury from Mount Etna volcano (Southern Italy), Atmospheric Environment, 41, 7377–7388, https://doi.org/10.1016/j.atmosenv.2007.05.060, 2007.

Bagnato, E., Tamburello, G., Avard, G., Martinez Cruz, M., Enrico, M., Fu, X., Sprovieri, M., and Sonke, J.: Mercury fluxes from volcanic and geothermal sources: An update, Geological Society London Special Publications, 410, https://doi.org/10.1144/SP410.2, 2014.

Bekki, S.: Oxidation of volcanic SO2: A sink for stratospheric OH and H2O, Geophysical Research Letters, 22, 913–916, https://doi.org/10.1029/95gl00534, 1995.

Bobrowski, N. and Giuffrida, G.: Bromine monoxide / sulphur dioxide ratios in relation to volcanological observations at Mt. Etna 2006 –2009, Solid Earth, 3, 433–445, https://doi.org/10.5194/se-3-433-2012, 2012.

Bobrowski, N., Hönninger, G., Galle, B., and Platt, U.: Detection of bromine monoxide in a volcanic plume, Nature, 423, 273–276, https://doi.org/10.1038/nature01625, 2003.

Bobrowski, N., von Glasow, R., Aiuppa, A., Inguaggiato, S., Louban, I., Ibrahim, O. W., and Platt, U.: Reactive halogen chemistry in volcanic plumes, Journal of Geophysical Research-Atmospheres, 112, https://doi.org/10.1029/2006jd007206, 2007.

Bobrowski, N., von Glasow, R., Giuffrida, G. B., Tedesco, D., Aiuppa, A., Yalire, M., Arellano, S., Johansson, M., and Galle, B.: Gas emission strength and evolution of the molar ratio of BrO/SO2in the plume of Nyiragongo in comparison to Etna, Journal of Geophysical Research: Atmospheres, 120, 277–291, https://doi.org/10.1002/2013jd021069, 2015.

Bobrowski, N., Giuffrida, G. B., Arellano, S., Yalire, M., Liotta, M., Brusca, L., Calabrese, S., Scaglione, S., Rüdiger, J., Castro, J. M., Galle, B., and Tedesco, D.: Plume composition and volatile flux of Nyamulagira volcano, Democratic Republic of Congo, during birth and evolution of the lava lake, 2014–2015, Bulletin of Volcanology, 79, https://doi.org/10.1007/s00445-017-1174-0, 2017.

Brenna, H., Kutterolf, S., Mills, M. J., and Krüger, K.: The potential impacts of a sulfur- and halogen-rich supereruption such as Los Chocoyos on the atmosphere and climate, Atmospheric Chemistry and Physics, 20, 6521–6539, https://doi.org/10.5194/acp-20-6521-2020, 2020.

Buchholz, R. R., Emmons, L. K., Tilmes, S., and The CESM2 Development Team: CESM2.1/CAM-chem Instantaneous Output for Boundary Conditions - Subset used: 20°N–45°N, 5°E–45°E 2018-12-21–2018-12-29, Accessed: 10-12-2019, https://doi.org/10.5065/NMP7-EP60, https://wiki.ucar.edu/display/camchem/CESM2.1:CAM-chem+as+Boundary+Conditions, 2019.

Burton, R. R., Woodhouse, M. J., Gadian, A. M., and Mobbs, S. D.: The Use of a Numerical Weather Prediction Model to Simulate Near-Field Volcanic Plumes, Atmosphere, 11, 594, https://doi.org/10.3390/atmos11060594, 2020.

Cadoux, A., Scaillet, B., Bekki, S., Oppenheimer, C., and Druitt, T. H.: Stratospheric Ozone destruction by the Bronze-Age Minoan eruption (Santorini Volcano, Greece), Scientific Reports, 5, https://doi.org/10.1038/srep12243, 2015.

Carn, S., Clarisse, L., and Prata, A.: Multi-decadal satellite measurements of global volcanic degassing, Journal of Volcanology and Geothermal Research, 311, 99–134, https://doi.org/10.1016/j.jvolgeores.2016.01.002, 2016.

Dinger, F., Bobrowski, N., Warnach, S., Bredemeyer, S., Hidalgo, S., Arellano, S., Galle, B., Platt, U., and Wagner, T.: Periodicity in the BrO/SO_2 molar ratios in the volcanic gas plume of Cotopaxi and its correlation with the Earth tides during the eruption in 2015, Solid Earth, 9, 247–266, https://doi.org/10.5194/se-9-247-2018, 2018.

Dinger, F., Kleinbek, T., Dörner, S., Bobrowski, N., Platt, U., Wagner, T., Ibarra, M., and Espinoza, E.: SO_2 and BrO emissions of Masaya volcano from 2014–2020, Atmospheric Chemistry and Physics Discussions, 2020, 1–49, https://doi.org/10.5194/acp-2020-942, 2020.

Egan, S. D., Stuefer, M., Webley, P. W., Lopez, T., Cahill, C. F., and Hirtl, M.: Modeling volcanic ash aggregation processes and related impacts on the April–May 2010 eruptions of Eyjafjallajökull volcano with WRF-Chem, Natural Hazards and Earth System Sciences, 20, 2721–2737, https://doi.org/10.5194/nhess-20-2721-2020, 2020.

Emmons, L. K., Schwantes, R. H., Orlando, J. J., Tyndall, G., Kinnison, D., Lamarque, J.-F., Marsh, D., Mills, M. J., Tilmes, S., Bardeen, C., Buchholz, R. R., Conley, A., Gettelman, A., Garcia, R., Simpson, I., Blake, D. R., Meinardi, S., and Pétron, G.: The Chemistry Mechanism in the Community Earth System Model version 2 (CESM2), Journal of Advances in Modeling Earth Systems, p. e2019MS001882, 2020.

Freitas, S. R., Longo, K. M., Alonso, M. F., Pirre, M., Marecal, V., Grell, G., Stockler, R., Mello, R. F., and Sánchez Gácita, M.: PREP-CHEM-SRC – 1.0: a preprocessor of trace gas and aerosol emission fields for regional and global atmospheric chemistry models, Geoscientific Model Development, 4, 419–433, https://doi.org/10.5194/gmd-4-419-2011, 2011.

Galeazzo, T., Bekki, S., Martin, E., Savarino, J., and Arnold, S. R.: Photochemical box modelling of volcanic SO2 oxidation: isotopic constraints, Atmospheric Chemistry and Physics, 18, 17 909–17 931, https://doi.org/10.5194/acp-18-17909-2018, 2018.

General, S., Bobrowski, N., Pöhler, D., Weber, K., Fischer, C., and Platt, U.: Airborne I-DOAS measurements at Mt. Etna: BrO and OClO evolution in the plume, Journal of Volcanology and Geothermal Research, https://doi.org/10.1016/j.jvolgeores.2014.05.012, in press, 2014.

Gerlach, T. M.: Volcanic sources of tropospheric ozone-depleting trace gases, Geochemistry Geophysics Geosystems, 5, https://doi.org/10.1029/2004gc000747, 2004.

Gliß, J., Bobrowski, N., Vogel, L., Pöhler, D., and Platt, U.: OClO and BrO observations in the volcanic plume of Mt. Etna – implications on the chemistry of chlorine and bromine species in volcanic plumes, Atmospheric Chemistry and Physics, 15, 5659–5681, https://doi.org/10.5194/acp-15-5659-2015, 2015.

Grell, G. A., Peckham, S. E., Schmitz, R., McKeen, S. A., Frost, G., Skamarock, W. C., and Eder, B.: Fully coupled "online" chemistry within the WRF model, Atmospheric Environment, 39, 6957–6975, https://doi.org/10.1016/j.atmosenv.2005.04.027, 2005.

Gutmann, A., Bobrowski, N., Roberts, T. J., Rüdiger, J., and Hoffmann, T.: Advances in Bromine Speciation in Volcanic Plumes, Frontiers in Earth Science, 6, 213, https://doi.org/10.3389/feart.2018.00213, 2018.

Hirtl, M., Stuefer, M., Arnold, D., Grell, G., Maurer, C., Natali, S., Scherllin-Pirscher, B., and Webley, P.: The effects of simulating volcanic aerosol radiative feedbacks with WRF-Chem during the Eyjafjallajökull eruption, April and May 2010, Atmospheric Environment, 198, 194–206, https://doi.org/10.1016/j.atmosenv.2018.10.058, 2019.

Hirtl, M., Scherllin-Pirscher, B., Stuefer, M., Arnold, D., Baro, R., Maurer, C., and Mulder, M. D.: Extension of the WRF-Chem volcanic emission preprocessor to integrate complex source terms and evaluation for different emission scenarios of the Grimsvötn 2011 eruption, Natural Hazards and Earth System Sciences, 20, 3099–3115, https://doi.org/10.5194/nhess-20-3099-2020, 2020.

Hörmann, C., Sihler, H., Bobrowski, N., Beirle, S., Penning de Vries, M., Platt, U., and Wagner, T.: Systematic investigation of bromine monoxide in volcanic plumes from space by using the GOME-2 instrument, Atmospheric Chemistry and Physics, 13, 4749–4781, https://doi.org/10.5194/acp-13-4749-2013, 2013.

Jourdain, L., Roberts, T. J., Pirre, M., and Josse, B.: Modeling the reactive halogen plume from Ambrym and its impact on the troposphere with the CCATT-BRAMS mesoscale model, Atmospheric Chemistry and Physics, 16, 12 099–12 125, https://doi.org/10.5194/acp-16-12099-2016, 2016.

Kelly, P. J., Kern, C., Roberts, T. J., Lopez, T., Werner, C., and Aiuppa, A.: Rapid chemical evolution of tropospheric volcanic emissions from Redoubt Volcano, Alaska, based on observations of ozone and halogen-containing gases, Journal of Volcanology and Geothermal Research, 259, 317–333, https://doi.org/10.1016/j.jvolgeores.2012.04.023, 2013.

Klobas, J. E., Wilmouth, D. M., Weisenstein, D. K., Anderson, J. G., and Salawitch, R. J.: Ozone depletion following future volcanic eruptions, Geophysical Research Letters, 44, 7490–7499, https://doi.org/10.1002/2017GL073972, 2017.

Kutterolf, S., Hansteen, T., Appel, K., Freundt, A., Krğer, K., Pérez, W., and Wehrmann, H.: Combined bromine and chlorine release from large explosive volcanic eruptions: A threat to stratospheric ozone?, Geology, 41, 707–710, https://doi.org/10.1130/G34044.1, 2013.

Lachatre, M., Mailler, S., Menut, L., Turquety, S., Sellitto, P., Guermazi, H., Salerno, G., Caltabiano, T., and Carboni, E.: New strategies for vertical transport in chemistry transport models: application to the case of the Mount Etna eruption on 18 March 2012 with CHIMERE v2017r4, Geoscientific Model Development, 13, 5707–5723, https://doi.org/10.5194/gmd-13-5707-2020, 2020.

Lurton, T., Jégou, F., Berthet, G., Renard, J.-B., Clarisse, L., Schmidt, A., Brogniez, C., and Roberts, T. J.: Model simulations of the chemical and aerosol microphysical evolution of the Sarychev Peak 2009 eruption cloud compared to in situ and satellite observations, Atmospheric Chemistry and Physics, 18, 3223–3247, https://doi.org/10.5194/acp-18-3223-2018, 2018.

Marelle, L., Thomas, J. L., Ahmed, S., Tuite, K., Stutz, J., Dommergue, A., Simpson, W. R., and Frey., M. M.: Implementation and impacts of surface and blowing snow sources of Arctic bromine activation within WRF-Chem, Journal of Advances in Modeling Earth Systems, in review.

Martin, R. S., Ilyinskaya, E., and Oppenheimer, C.: The enigma of reactive nitrogen in volcanic emissions, Geochimica et Cosmochimica Acta, 95, 93–105, https://doi.org/10.1016/j.gca.2012.07.027, 2012.

Maters, E. C., Delmelle, P., Rossi, M. J., and Ayris, P. M.: Reactive Uptake of Sulfur Dioxide and Ozone on Volcanic Glass and Ash at Ambient Temperature, Journal of Geophysical Research: Atmospheres, 122, 10,077–10,088, https://doi.org/10.1002/2017JD026993, 2017.

Mather, T., Allen, A., Davison, B., Pyle, D., Oppenheimer, C., and McGonigle, A.: Nitric acid from volcanoes, Earth and Planetary Science Letters, 218, 17 – 30, https://doi.org/10.1016/S0012-821X(03)00640-X, 2004a.

Mather, T. A.: Volcanoes and the environment: Lessons for understanding Earth's past and future from studies of present-day volcanic emissions, Journal of Volcanology and Geothermal Research, 304, 160–179, https://doi.org/10.1016/j.jvolgeores.2015.08.016, 2015.

Mather, T. A., Pyle, D. M., and Allen, A. G.: Volcanic source for fixed nitrogen in the early Earth's atmosphere, Geology, 32, 905–908, https://doi.org/10.1130/G20679.1, 2004b.

Millard, G. A., Mather, T. A., Pyle, D. M., Rose, W. I., and Thornton, B.: Halogen emissions from a small volcanic eruption: Modeling the peak concentrations, dispersion, and volcanically induced ozone loss in the stratosphere, Geophysical Research Letters, 33, https://doi.org/10.1029/2006GL026959, 2006.

Ming, A., Winton, V. H. L., Keeble, J., Abraham, N. L., Dalvi, M. C., Griffiths, P., Caillon, N., Jones, A. E., Mulvaney, R., Savarino, J., Frey, M. M., and Yang, X.: Stratospheric Ozone Changes From Explosive Tropical Volcanoes: Modeling and Ice Core Constraints, Journal of Geophysical Research: Atmospheres, 125, e2019JD032 290, https://doi.org/10.1029/2019JD032290, 2020.

National Centers for Environmental Prediction, National Weather Service, NOAA, and U.S. Department of Commerce: NCEP FNL Operational Model Global Tropospheric Analyses, continuing from July 1999 - accessed 2019, https://doi.org/10.5065/D6M043C6, 2000.

Oppenheimer, C., Kyle, P., Eisele, F., Crawford, J., Huey, G., Tanner, D., Kim, S., Mauldin, L., Blake, D., Beyersdorf, A., Buhr, M., and Davis, D.: Atmospheric chemistry of an Antarctic volcanic plume, Journal of Geophysical Research-Atmospheres, 115, https://doi.org/10.1029/2009jd011910, 2010.

Oppenheimer, C., Scaillet, B., and Martin, R. S.: Sulfur Degassing From Volcanoes: Source Conditions, Surveillance, Plume Chemistry and Earth System Impacts, Reviews in Mineralogy and Geochemistry, 73, 363–421, https://doi.org/10.2138/rmg.2011.73.13, 2011.

Prata, A. J., Carn, S. A., Stohl, A., and Kerkmann, J.: Long range transport and fate of a stratospheric volcanic cloud from Soufrière Hills volcano, Montserrat, Atmospheric Chemistry and Physics, 7, 5093–5103, https://doi.org/10.5194/acp-7-5093-2007, 2007.

Pyle, D. and Mather, T.: Halogens in igneous processes and their fluxes to the atmosphere and oceans from volcanic activity: A review, Chemical Geology, 263, 110–121, https://doi.org/10.1016/j.chemgeo.2008.11.013, 2009.

Pyle, D. M. and Mather, T. A.: The importance of volcanic emissions for the global atmospheric mercury cycle, Atmospheric Environment, 37, 5115 – 5124, https://doi.org/10.1016/j.atmosenv.2003.07.011, 2003.

Rizza, U., Brega, E., Caccamo, M. T., Castorina, G., Morichetti, M., Munaò, G., Passerini, G., and Magazù, S.: Analysis of the ETNA 2015 Eruption Using WRF–Chem Model and Satellite Observations, Atmosphere, 11, https://doi.org/10.3390/atmos11111168, 2020.

Roberts, T.: Ozone Depletion in Tropospheric Volcanic Plumes: From Halogen-Poor to Halogen-Rich Emissions, Geosciences, 8, 68, https://doi.org/10.3390/geosciences8020068, 2018.

Roberts, T., Vignelles, D., Liuzzo, M., Giudice, G., Aiuppa, A., Coltelli, M., Salerno, G., Chartier, M., Couté, B., Berthet, G., Lurton, T., Dulac, F., and Renard, J.-B.: The primary volcanic aerosol emission from Mt Etna: Size-resolved particles with SO2 and role in plume reactive halogen chemistry, Geochimica et Cosmochimica Acta, 222, 74–93, https://doi.org/10.1016/j.gca.2017.09.040, 2018.

Roberts, T., Dayma, G., and Oppenheimer, C.: Reaction Rates Control High-Temperature Chemistry of Volcanic Gases in Air, Frontiers in Earth Science, 7, 154, https://doi.org/10.3389/feart.2019.00154, 2019.

Roberts, T. J., Braban, C. F., Martin, R. S., Oppenheimer, C., Adams, J. W., Cox, R. A., Jones, R. L., and Griffiths, P. T.: Modelling reactive halogen formation and ozone depletion in volcanic plumes, Chemical Geology, 263, 151–163, https://doi.org/10.1016/j.chemgeo.2008.11.012, 2009.

Roberts, T. J., Martin, R. S., and Jourdain, L.: Reactive bromine chemistry in Mount Etna's volcanic plume: the influence of total Br, high-temperature processing, aerosol loading and plume–air mixing, Atmospheric Chemistry and Physics, 14, 11 201–11 219, https://doi.org/10.5194/acp-14-11201-2014, 2014.

Rose, W. I., Millard, G. A., Mather, T. A., Hunton, D. E., Anderson, B., Oppenheimer, C., Thornton, B. F., Gerlach, T. M., Viggiano, A. A., Kondo, Y., Miller, T. M., and Ballenthin, J. O.: Atmospheric chemistry of a 33–34 hour old volcanic cloud from Hekla Vol-

cano (Iceland): Insights from direct sampling and the application of chemical box modeling, Journal of Geophysical Research, 111, https://doi.org/10.1029/2005jd006872, 2006.

Rüdiger, J., Bobrowski, N., Liotta, M., and Hoffmann, T.: Development and application of a sampling method for the determination of reactive halogen species in volcanic gas emissions, Analytical and Bioanalytical Chemistry, 409, 5975–5985, https://doi.org/10.1007/s00216-017-0525-1, 2017.

Rüdiger, J., Gutmann, A., Bobrowski, N., Liotta, M., de Moor, J. M., Sander, R., Dinger, F., Tirpitz, J.-L., Ibarra, M., Saballos, A., Martínez, M., Mendoza, E., Ferrufino, A., Stix, J., Valdés, J., Castro, J. M., and Hoffmann, T.: Halogen activation in the plume of Masaya volcano: field observations and box model investigations, Atmospheric Chemistry and Physics Discussions, https://doi.org/10.5194/acp-2020-284, 2020.

Saiz-Lopez, A., Sitkiewicz, S. P., Roca-Sanjuán, D., Oliva-Enrich, J. M., Dávalos, J. Z., Notario, R., Jiskra, M., Xu, Y., Wang, F., Thackray, C. P., Sunderland, E. M., Jacob, D. J., Travnikov, O., Cuevas, C. A., Acuña, A. U., Rivero, D., Plane, J. M. C., Kinnison, D. E., and Sonke, J. E.: Photoreduction of gaseous oxidized mercury changes global atmospheric mercury speciation, transport and deposition, Nature Communications, 9, https://doi.org/10.1038/s41467-018-07075-3, 2018.

Saiz-Lopez, A., Acuña, A. U., Trabelsi, T., Carmona-García, J., Dávalos, J. Z., Rivero, D., Cuevas, C. A., Kinnison, D. E., Sitkiewicz, S. P., Roca-Sanjuán, D., and Francisco, J. S.: Gas-Phase Photolysis of Hg(I) Radical Species: A New Atmospheric Mercury Reduction Process, Journal of the American Chemical Society, 141, 8698–8702, https://doi.org/10.1021/jacs.9b02890, 2019.

Salerno, G., Burton, M., Oppenheimer, C., Caltabiano, T., Randazzo, D., Bruno, N., and Longo, V.: Three-years of SO_2 flux measurements of Mt. Etna using an automated UV scanner array: Comparison with conventional traverses and uncertainties in flux retrieval, Journal of Volcanology and Geothermal Research, 183, 76–83, https://doi.org/10.1016/j.jvolgeores.2009.02.013, 2009.

Seigneur, C. and Lohman, K.: Effect of bromine chemistry on the atmospheric mercury cycle, Journal of Geophysical Research: Atmospheres, 113, D23309, https://doi.org/10.1029/2008JD010262, 2008.

Seigneur, C., Vijayaraghavan, K., and Lohman, K.: Atmospheric mercury chemistry: Sensitivity of global model simulations to chemical reactions, Journal of Geophysical Research, 111, D22306, https://doi.org/10.1029/2005jd006780, 2006.

Seo, S., Richter, A., Blechschmidt, A.-M., Bougoudis, I., and Burrows, J. P.: First high-resolution BrO column retrievals from TROPOMI, Atmospheric Measurement Techniques, 12, 2913–2932, https://doi.org/10.5194/amt-12-2913-2019, 2019.

Staunton-Sykes, J., Aubry, T. J., Shin, Y. M., Weber, J., Marshall, L. R., Luke Abraham, N., Archibald, A., and Schmidt, A.: Co-emission of volcanic sulfur and halogens amplifies volcanic effective radiative forcing, Atmospheric Chemistry and Physics, 21, 9009–9029, https://doi.org/10.5194/acp-21-9009-2021, 2021.

Stuefer, M., Freitas, S. R., Grell, G., Webley, P., Peckham, S., McKeen, S. A., and Egan, S. D.: Inclusion of ash and SO_2 emissions from volcanic eruptions in WRF-Chem: development and some applications, Geoscientific Model Development, 6, 457–468, https://doi.org/10.5194/gmd-6-457-2013, 2013.

Surl, L.: Modelling the atmospheric chemistry of volcanic plumes, Ph.D. thesis, University of East Anglia, https://ueaeprints.uea.ac.uk/id/eprint/59407/, 2016.

Surl, L.: WRF-Chem Volcano [software], https://github.com/LukeSurl/WCV, 2020.

Surl, L.: WRF-Chem Volcano output - Etna Summer 2012 [dataset], https://doi.org/10.5281/zenodo.4415788, 2021.

Surl, L., Donohoue, D., Aiuppa, A., Bobrowski, N., and von Glasow, R.: Quantification of the depletion of ozone in the plume of Mount Etna, Atmospheric Chemistry and Physics, 15, 2613–2628, https://doi.org/10.5194/acp-15-2613-2015, 2015.

Theys, N., Van Roozendael, M., Dils, B., Hendrick, F., Hao, N., and De Mazière, M.: First satellite detection of volcanic bromine monoxide emission after the Kasatochi eruption, Geophysical Research Letters, 36, https://doi.org/10.1029/2008GL036552, 2009.

Theys, N., De Smedt, I., Van Roozendael, M., Froidevaux, L., Clarisse, L., and Hendrick, F.: First satellite detection of volcanic OClO after the eruption of Puyehue-Cordón Caulle, Geophysical Research Letters, 41, 667–672, https://doi.org/10.1002/2013GL058416, 2014.

Vance, A., McGonigle, A. J. S., Aiuppa, A., Stith, J. L., Turnbull, K., and von Glasow, R.: Ozone depletion in tropospheric volcanic plumes, Geophysical Research Letters, 37, https://doi.org/10.1029/2010GL044997, 2010.

Voigt, C., Jessberger, P., Jurkat, T., Kaufmann, S., Baumann, R., Schlager, H., Bobrowski, N., Giuffrida, G., and Salerno, G.: Evolution of CO2, SO2, HCl, and HNO3in the volcanic plumes from Etna, Geophysical Research Letters, 41, 2196–2203, https://doi.org/10.1002/2013gl058974, 2014.

von Glasow, R.: Atmospheric chemistry in volcanic plumes, Proceedings of the National Academy of Sciences, 107, 6594–6599, https://doi.org/10.1073/pnas.0913164107, 2010.

von Glasow, R., Bobrowski, N., and Kern, C.: The effects of volcanic eruptions on atmospheric chemistry, Chemical Geology, 263, 131–142, https://doi.org/10.1016/j.chemgeo.2008.08.020, 2009.

Wade, D. C., Vidal, C. M., Abraham, N. L., Dhomse, S., Griffiths, P. T., Keeble, J., Mann, G., Marshall, L., Schmidt, A., and Archibald, A. T.: Reconciling the climate and ozone response to the 1257 CE Mount Samalas eruption, Proceedings of the National Academy of Sciences, 117, 26 651–26 659, https://doi.org/10.1073/pnas.1919807117, 2020.

Warnach, S., Bobrowski, N., Hidalgo, S., Arellano, S., Sihler, H., Dinger, F., Lübcke, P., Battaglia, J., Steele, A., Galle, B., Platt, U., and Wagner, T.: Variation of the BrO/SO2 Molar Ratio in the Plume of Tungurahua Volcano Between 2007 and 2017 and Its Relationship to Volcanic Activity, Frontiers in Earth Science, 7, https://doi.org/10.3389/feart.2019.00132, 2019.

Weigelt, A., Ebinghaus, R., Pirrone, N., Bieser, J., Bödewadt, J., Esposito, G., Slemr, F., van Velthoven, P. F. J., Zahn, A., and Ziereis, H.: Tropospheric mercury vertical profiles between 500 and 10,000 m in central Europe, Atmospheric Chemistry and Physics, 16, 4135–4146, https://doi.org/10.5194/acp-16-4135-2016, 2016a.

Weigelt, A., Slemr, F., Ebinghaus, R., Pirrone, N., Bieser, J., Bödewadt, J., Esposito, G., and van Velthoven, P. F. J.: Mercury emissions of a coal-fired power plant in Germany, Atmospheric Chemistry and Physics, 16, 13 653–13 668, https://doi.org/10.5194/acp-16-13653-2016, 2016b.

Wennberg, P.: Atmospheric chemistry - Bromine explosion, Nature, 397, 299, https://doi.org/10.1038/16805, 1999.

Wild, O., Zhu, X., and Prather, M. J.: Fast-J: Accurate Simulation of In- and Below-Cloud Photolysis in Tropospheric Chemical Models, Journal of Atmospheric Chemistry, 37, 245–282, https://doi.org/10.1023/a:1006415919030, 2000.

Witt, M. L. I., Mather, T. A., Pyle, D. M., Aiuppa, A., Bagnato, E., and Tsanev, V. I.: Mercury and halogen emissions from Masaya and Telica volcanoes, Nicaragua, Journal of Geophysical Research: Solid Earth, 113, https://doi.org/10.1029/2007JB005401, 2008.

Wittmer, J., Bobrowski, N., Liotta, M., Giuffrida, G., Calabrese, S., and U., P.: Active alkaline traps to determine acidic-gas ratios in volcanic plumes: sampling technique and analytical Methods, Geochem. Geophys. Geosyst, https://doi.org/10.1002/2013GC005133, 2014.

Zaveri, R. A. and Peters, L. K.: A new lumped structure photochemical mechanism for large-scale applications, Journal of Geophysical Research: Atmospheres, 104, 30 387–30 415, https://doi.org/10.1029/1999JD900876, 1999.

Zaveri, R. A., Easter, R. C., Fast, J. D., and Peters, L. K.: Model for Simulating Aerosol Interactions and Chemistry (MOSAIC), Journal of Geophysical Research: Atmospheres, 113, https://doi.org/10.1029/2007JD008782, 2008.